INNATE IMMUNITY

GTF3A mutations predispose to herpes simplex encephalitis by disrupting biogenesis of the host-derived RIG-I ligand *RNA5SP141*

Leslie Naesens[1,2,3]†, Santoshi Muppala[3]†, Dhiraj Acharya[3,4], Josephine Nemegeer[5,6], Delfien Bogaert[1,2], Jung-Hyun Lee[3,4]‡, Katrien Staes[5], Veronique Debacker[1,2], Pieter De Bleser[5,7], Marieke De Bruyne[8,9], Elfride De Baere[8,9], Michiel van Gent[3,4]§, GuanQun Liu[3,4], Bart N. Lambrecht[1,10], Jens Staal[5,11], Tessa Kerre[1,12], Rudi Beyaert[5,11], Jonathan Maelfait[5,6]||, Simon J. Tavernier[2,5,8,9,11]||, Michaela U. Gack[3,4]||*, Filomeen Haerynck[1,2]||*

Herpes simplex virus 1 (HSV-1) infects several billion people worldwide and can cause life-threatening herpes simplex encephalitis (HSE) in some patients. Monogenic defects in components of the type I interferon system have been identified in patients with HSE, emphasizing the role of inborn errors of immunity underlying HSE pathogenesis. Here, we identify compound heterozygous loss-of-function mutations in the gene *GTF3A* encoding for transcription factor IIIA (TFIIIA), a component of the RNA polymerase III complex, in a patient with common variable immunodeficiency and HSE. Patient fibroblasts and *GTF3A* gene–edited cells displayed impaired HSV-1–induced innate immune responses and enhanced HSV-1 replication. Chromatin immunoprecipitation sequencing analysis identified the 5*S* ribosomal RNA pseudogene 141 (*RNA5SP141*), an endogenous ligand of the RNA sensor RIG-I, as a transcriptional target of TFIIIA. *GTF3A* mutant cells exhibited diminished *RNA5SP141* expression and abrogated RIG-I activation upon HSV-1 infection. Our work unveils a crucial role for TFIIIA in transcriptional regulation of a cellular RIG-I agonist and shows that *GTF3A* genetic defects lead to impaired cell-intrinsic anti–HSV-1 responses and can predispose to HSE.

INTRODUCTION

Herpes simplex virus 1 (HSV-1) is one of the most common human pathogens, infecting several billion people worldwide (*1*). HSV-1 is primarily transmitted through oral-to-oral contact and commonly causes mild mucocutaneous infections. However, in rare cases (1 in 250,000 to 500,000 individuals per year), the virus causes herpes simplex encephalitis (HSE) predominantly in children younger than 3 years old (*2*). Late diagnosis of HSE or lack of adequate antiviral therapy is associated with high mortality (~70%), and most survivors develop neurological sequelae (*2*).

The host innate immune surveillance machinery plays a crucial role in the defense against HSV-1 and dictates the outcome of infection (*3*). Nucleic acid sensors survey different cellular compartments for viral or cellular RNA or DNA ligands and induce the production of type I interferons (IFN-I), proinflammatory cytokines, and chemokines (*4*). Studies in cell culture and/or in mice have shown that different classes of nucleic acid receptors contribute to the sensing of HSV-1 infection, including Toll-like receptors (e.g., TLR3 and TLR9) and the intracellular sensors cGAS and IFI16 (*5*). Human studies demonstrated the importance of the double-stranded RNA (dsRNA) sensor TLR3 in restricting HSV-1 replication and pathogenesis by mediating constitutive IFN-I immunity (*6*, *7*). Accumulating evidence from in vitro experiments using a variety of cell types showed that the cytoplasmic RNA sensor RIG-I, which signals through MAVS (mitochondrial antiviral signaling protein), also critically contributes to the innate immune response to HSV-1 and other herpesviruses such as varicella-zoster virus (VZV), Epstein-Barr virus (EBV), and Kaposi's sarcoma–associated herpesvirus (KSHV) (*8*, *9*). RNA polymerase III (Pol III) has been shown to convert host- or virus-derived DNA products into 5′-triphosphate RNA ligands for RIG-I (*10*, *11*). RIG-I affinity purification from HSV-1–infected cells and next-generation sequencing of bound RNA revealed that small noncoding RNAs, in particular the 5*S* ribosomal pseudogene transcript *RNA5SP141* (5*S* ribosomal RNA pseudogene 141), serve as RIG-I cellular ligands (*12*).

Inborn errors in genes implicated in TLR3 nucleic acid sensing or in downstream signaling components (*UNC93B1*, *TLR3*, *TRIF*, *TRAF3*, *TBK1*, or *IRF3*) account for ~5% of HSE cases (*7*). Two recent studies revealed genetic defects in TLR3-independent antiherpesviral mechanisms, including autosomal recessive *DBR1*

[1]Department of Internal Medicine and Pediatrics, Ghent University, Ghent, Belgium. [2]Primary Immunodeficiency Research Lab, Center for Primary Immunodeficiency, Jeffrey Modell Diagnosis and Research Center, Ghent University Hospital, Ghent, Belgium. [3]Florida Research and Innovation Center, Cleveland Clinic, Port St. Lucie, FL, USA. [4]Department of Microbiology, University of Chicago, Chicago, IL, USA. [5]Department of Biomedical Molecular Biology, Ghent University, Ghent, Belgium. [6]Laboratory of Molecular Signaling and Cell death, VIB-UGent Center for Inflammation Research, Ghent, Belgium. [7]Laboratory of Data Mining and Modeling for Biomedicine, VIB-UGent Center for Inflammation Research, Ghent, Belgium. [8]Department of Biomolecular Medicine, Ghent University, Ghent, Belgium. [9]Center for Medical Genetics, Ghent University Hospital, Ghent, Belgium. [10]Laboratory of Immunoregulation and Mucosal Immunology, VIB-UGent Center for Inflammation Research, Ghent, Belgium. [11]Laboratory of Molecular Signal Transduction in Inflammation, VIB-UGent Center for Inflammation Research, Ghent, Belgium. [12]Department of Hematology, Jeffrey Modell Diagnosis and Research Center, Ghent University Hospital, Ghent, Belgium.
*Corresponding author. Email: gackm@ccf.org (M.U.G.); filomeen.haerynck@uzgent.be (F.H.)
†These authors contributed equally to this work.
‡Present address: Department of Life Science, University of Seoul, Seoul, Republic of Korea.
§Present address: Department of Viroscience, Erasmus Medical Center, Rotterdam, Netherlands.
||These authors contributed equally to this work.

deficiency and heterozygous mutations in *SNORA31* for which the molecular antiviral mechanism(s) remains to be elucidated (*13*, *14*). To date, for many HSE cases, the underlying genetic defects are still unknown.

Here, we identify a role for loss-of-function (LOF) mutations in *GTF3A*, encoding for transcription factor IIIA (TFIIIA), which is part of the Pol III complex, in HSE. Our work shows that TFIIIA induces the expression of the RIG-I ligand *RNA5SP141*, thereby enabling protective IFN-I–mediated immunity against HSV-1 infection, which is abrogated in cells harboring *GTF3A* mutations.

RESULTS

Compound heterozygous *GTF3A* mutations in a patient with common variable immunodeficiency and HSE

We investigated a nonconsanguineous Belgian family in which the proband exhibited a common variable immunodeficiency (CVID) phenotype including susceptibility to bacterial upper respiratory infections, hypogammaglobulinemia, absent immunoglobulin M (IgM), and defective pneumococcal antibody responses requiring intravenous Ig replacement treatment (detailed case descriptions and laboratory immunologic evaluation are included in fig. S1, A to G, and table S1). Immunophenotyping revealed increased transitional B cells, low switched memory B cells, increased $CD21^-$ B cells, and T cell numbers around the lower limit of normal range during infancy, slowly improving with age (fig. S1, A and B). T cells displayed mostly a memory and effector phenotype (fig. S1, C and D). Evaluation of innate immune cells revealed no obvious defects. Plasmacytoid dendritic cell and natural killer cell percentages were within the normal range (fig. S1, E and F). Analysis of $CD4^+$ T cell subsets showed reduced percentages of T follicular helper cells and T helper 17 cells (fig. S1G), and T cells responded normally to mitogens (table S1). At the age of 9 months, the patient was hospitalized for HSE with positive HSV-1 polymerase chain reaction (PCR) testing on cerebrospinal fluid and responded well to intravenous treatment with acyclovir.

We performed whole-exome sequencing (WES) focusing on genetic susceptibility to viral infections because invasive HSV-1 infections are not commonly associated with CVID (*15*). WES analysis did not reveal pathogenic variants in known HSE-susceptibility genes (*UNC93B*, *TLR3*, *TRIF*, *TRAF3*, *TBK1*, *IRF3*, *IFNAR1*, and *DBR1*) nor in any other gene included in our in-house primary immunodeficiency disease screening panel. Sanger sequencing excluded variants in *SNORA31*, encoding a small nucleolar RNA that has been associated with HSE (*14*). We therefore searched for other candidate genes by considering variants with minor (<0.001) allele frequencies and predicted to be deleterious as defined by in silico analysis tools (CADD, PolyPhen-2, and SIFT). Given the inheritance pattern, we prioritized biallelic and de novo mutations. This revealed two substitutions in the gene *GTF3A* at nucleotides c.585T>G and c.655T>C, resulting in missense variants p.C195W and p.C219R, respectively (Fig. 1, A and B). Both variants are absent from the Genome Aggregation Database (gnomAD) as well as our in-house database (containing 12,500 exomes) and are predicted to be pathogenic according to in silico analysis tools (Fig. 1C and table S2). Familial segregation using Sanger sequencing confirmed compound heterozygosity in both the proband (II:2) and his sister (II:3), who also exhibited CVID-like adaptive immunological defects, some of which were notably different from the proband (Fig. 1, A and B; fig. S1; and table S1). She is HSV-1 seropositive and has no medical history of severe herpesviral infections, suggesting an autosomal recessive trait with incomplete penetrance for HSE (table S1). Incomplete penetrance is also common in IFN-I pathway deficiencies known to be associated with HSE (*16*).

GTF3A encodes general TFIIIA, whose role in transcriptional regulation of 5*S* ribosomal DNA (rDNA) genes [encoding 5*S* ribosomal RNA (rRNA)] has been well characterized (*17*–*19*). TFIIIA comprises nine zinc finger (ZF) domains, each containing two invariant pairs of cysteines and histidines coordinating one Zn^{2+} ion (Fig. 1D) (*20*). In both C195W and C219R TFIIIA variants, one of the two highly conserved Cys residues containing sulfhydryl groups capable of forming disulfide bonds and essential for ZF formation, is replaced by a bulky hydrophobic tryptophan or a positively charged arginine (Fig. 1, E and F). Metal-binding ZFs with substitutions for the Cys residues at C<u>X</u>HH or <u>X</u>CHH, as is the case in the C195W and C219R TFIIIA mutants, respectively (Fig. 1F), exhibit decreased affinity for Zn^{2+} by four- to fivefold compared with the wild-type (WT) CCHH motif (*21*, *22*).

GTF3A missense mutations lead to impaired DNA binding ability of TFIIIA

To examine the impact of the *GTF3A* missense mutations, we first analyzed *GTF3A* mRNA and TFIIIA protein expression in primary cells by quantitative PCR (qPCR) [reverse transcription qPCR (RT-qPCR)] and Western blotting, respectively. This showed that the *GTF3A* mRNA and TFIIIA protein expression levels in patient and carrier cells were comparable to those in healthy controls (HCs) (Fig. 1, G and H). Next, we analyzed the subcellular location of green fluorescent protein (GFP)–fused WT or mutant TFIIIA by confocal microscopy. We found that both WT TFIIIA and the mutants (C195W and C219R) were almost exclusively present in the nucleus and accumulated in the nucleolus, consistent with TFIIIA's role in ribosome biogenesis (fig. S2A) (*23*). Although quantitative flow cytometry–based image analysis showed slightly decreased numbers of GFP-positive nucleoli for both mutants compared with WT TFIIIA (fig. S2, B and C), both missense variants of TFIIIA did not show any noticeable mislocalization (fig. S2A).

The ZF motifs of TFIIIA primarily mediate sequence-specific recognition of 5*S* rDNA genes where TFIIIA binds to three distinct sequence elements (A-box, intermediate element, and C-box) located in the center of the gene, collectively called the internal control region (ICR) (fig. S2D) (*24*). Therefore, we evaluated binding of GFP-fused WT and mutant TFIIIA proteins (alone or in combination) to a DNA probe comprising the ICR of the 5*S* rDNA gene by electrophoretic mobility shift assay (EMSA). The ICR-binding ability of TFIIIA C195W was markedly impaired compared with WT TFIIIA, whereas complete abolishment of DNA binding was observed for TFIIIA C219R, similar to a TFIIIA mutant with deletion of ZF7 [ZF7 knockout (ZF7KO)] known to have abrogated DNA binding (Fig. 1, I to K) (*25*). Furthermore, the combination of mutant/WT protein in a 50:50 ratio did not exert a dominant-negative effect on the DNA binding ability of WT TFIIIA (Fig. 1, I and J).

Using the population database gnomAD v2.1.1, we studied the human genomic variation of the *GTF3A* gene (*26*). The LOEUF score of 1.6 suggests weak selection and that *GTF3A* is rather tolerant to heterozygous LOF variants. Nonetheless, gnomAD is devoid of homozygous truncating *GTF3A* variants with predicted LOF (*26*).

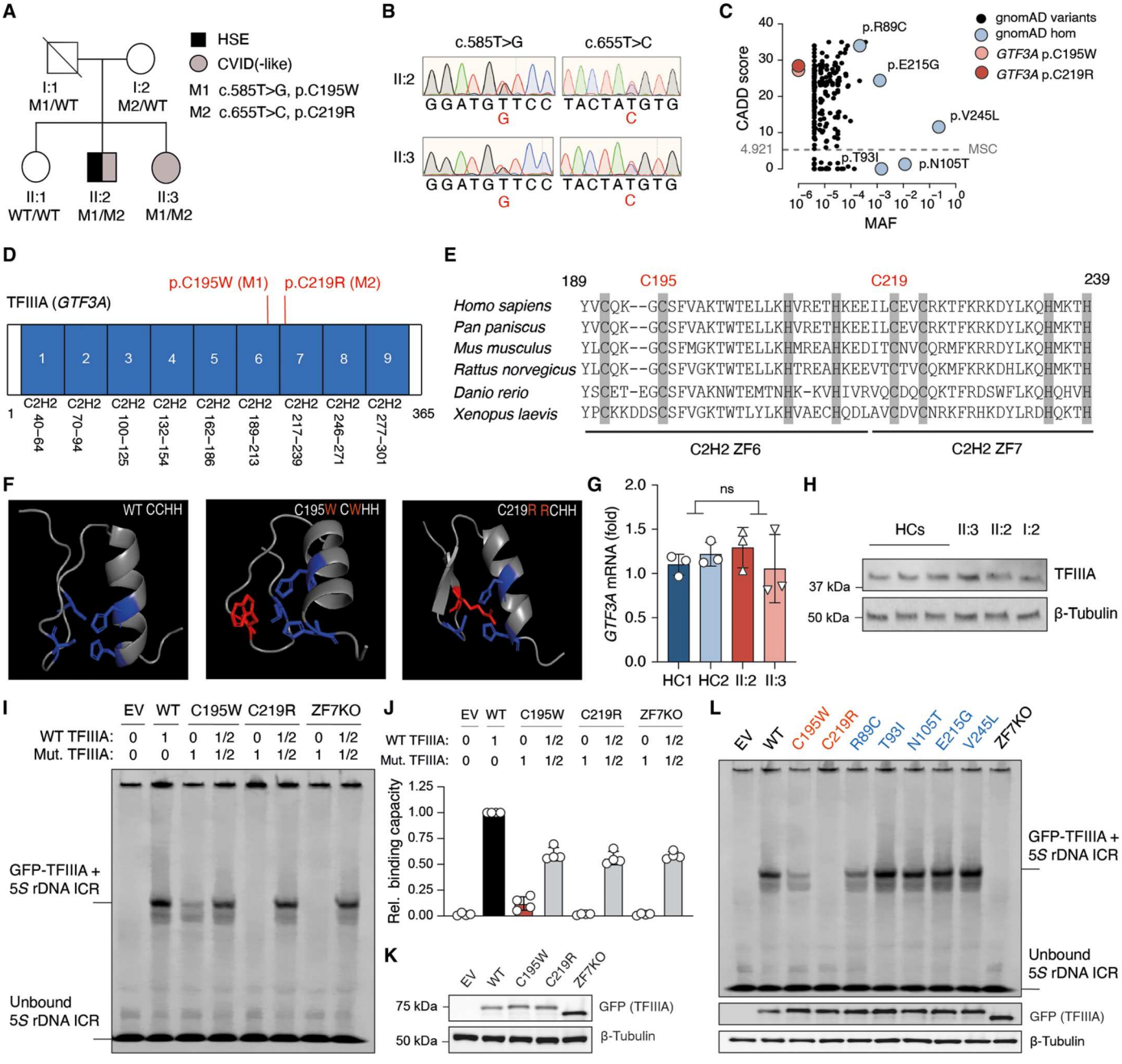

Fig. 1. Mutations in *GTF3A* result in impaired DNA binding ability in a patient with CVID and HSE. (**A**) Family pedigree with clinical phenotype and allele segregation of *GTF3A* variants. (**B**) Electropherograms of genomic DNA of primary fibroblasts from II:2 and II:3. (**C**) CADD score against minor allele frequency (MAF) for *GTF3A* variants in gnomAD with MSC (99% confidence interval) of 4.921. (**D**) Schematic of TFIIIA domain structure comprising nine C2H2 ZFs, with p.C195W and p.C219R mutations shown in red. Numbers below indicate amino acids. (**E**) Clustal Omega sequence alignment of TFIIIA (ZF6 and ZF7) from the indicated species, with conserved C2H2 residues shown in gray. Numbers above indicate amino acids. (**F**) Predicted 3D structure of the C2H2 ZFs of human TFIIIA protein (WT and mutants). Missense mutations (p.C195W and p.C219R) are shown in red. (**G**) RT-qPCR analysis of *GTF3A* expression in fibroblasts from II:2 and II:3 compared with HCs. (**H**) Endogenous TFIIIA protein expression in fibroblasts from HCs, II:2, II:3, and I:2, assessed by IB. (**I**) TFIIIA binding to 5*S* rDNA ICR assessed by EMSA on WCLs of HEK293T cells that were transfected for 16 hours with empty vector (EV) or GFP-fused TFIIIA WT, missense mutants (C195W and C219R), or ZF7KO (control) at indicated ratios. (**J**) Densitometric quantification of (I). (**K**) Expression of WT and mutant TFIIIA in the WCLs for (I), determined by IB. (**L**) TFIIIA binding to 5*S* rDNA ICR, determined by EMSA on WCLs of HEK293T cells that were transfected for 16 hours with EV or the indicated GFP-fused TFIIIA WT and mutant constructs. Each data point represents one biological replicate from three (G) or four (J) independent experiments (mean ± SD), or data shown are representative of at least two independent experiments (H, I, K, and L) (two-tailed, unpaired Student's *t* test). ns, statistically not significant.

gnomAD contains five homozygous missense variants: two with a CADD score below the mutation significance cutoff (MSC; 99% confidence interval) of 4.921 (T93I and N105T) and three variants with a high CADD score (R89C, E215G, and V245L). When tested for DNA binding, four of five variants (T93I, N105T, E215G, and V245L) showed comparable DNA binding as WT TFIIIA (Fig. 1L and fig. S2E). The TFIIIA R89C variant, introducing a Cys adjacent to the His residue of ZF2, had significantly impaired DNA binding comparable to that of the hypomorphic C195W mutant (Fig. 1L and fig. S2, E and F). Thus, most of the homozygous *GTF3A* variants are functionally normal.

Together, these results indicate that TFIIIA C195W and C219R mutant proteins exhibit normal nuclear localization but have impaired promoter-binding abilities. Complete *GTF3A* deficiency is not tolerated, and biallelic variants with severe LOF are very rare in the general population.

GTF3A mutant cells have impaired cell-intrinsic defense against HSV-1

We tested HSV-1 titers in unaffected carrier (II:3) and patient (II:2) fibroblasts harboring the compound heterozygous *GTF3A* mutations and found that these cells were highly susceptible to HSV-1 infection compared with cells from HCs (Fig. 2A). In accord, the expression of immediate early (*ICP0*), early (*ICP8*), and late (*UL36* and *gB*) HSV-1 genes was significantly increased in patient and carrier cells compared with HC cells (Fig. 2B). Reconstitution of the patient fibroblasts with WT TFIIIA reduced HSV-1 replication to similar levels as in HC cells (Fig. 2, C to E).

To corroborate the impact of the *GTF3A* missense mutations on viral control, we engineered human embryonic kidney (HEK) 293T knock-in (KI) clonal cell lines encoding TFIIIA C195W or C219R using CRISPR-Cas9 gene editing (fig. S3A). Expression of *GTF3A* mRNA and TFIIIA protein were normal in the homozygous TFIIIA C195W–expressing cell clones but reduced in the homozygous TFIIIA C219R clone (fig. S3, B to D). To mimic the compound heterozygous state of the *GTF3A* mutations, we also introduced the C195W substitution into a C219R clone containing a WT allele, thereby generating TFIIIA C195W/C219R KI cell clones (fig. S3A). We found significantly enhanced HSV-1 titers and viral transcripts in TFIIIA C195W/C219R KI cells and also in the respective homozygous TFIIIA C195W and C219R clones as compared with WT cells (Fig. 2, F and G, and fig. S3, E and F). Complementation of C195W/C219R KI cells with WT TFIIIA reduced viral gene expression (Fig. 2, H and I). Together, these results indicate that the identified *GTF3A* mutations lead to a loss of cell-intrinsic control of HSV-1 infection.

TFIIIA is a transcriptional regulator of the RIG-I ligand *RNA5SP141*

To elucidate the mechanism underlying TFIIIA's anti-herpesviral function, we searched for potential transcriptional targets of TFIIIA. Genomic mapping of the highly conserved ICR target sequence for TFIIIA using the Universal Robust Peak Annotation (UROPA) tool (*27*) identified 11 protein-coding genes and 122 noncoding RNAs (Fig. 3A and table S3). One of the predicted targets, *RIPK1*, is known to play a role in antiviral immunity (*28*), but its expression levels in *GTF3A* mutant fibroblasts and C195W/C219R HEK293T KI cells were comparable to those in control cells (fig. S4, A and B). The expression of 5SrRNA in the *GTF3A* mutant fibroblasts from carrier and patient was also comparable to that in control cells, similarly to what we observed for homozygous TFIIIA C195W KI cells (Fig. 3B and fig. S3D), suggesting complementary and/or compensatory mechanisms of its transcription. Further examination of the 116 genes with a centrally located ICR also revealed 5*S* rRNA pseudogenes (*RNA5SPs*), which have been recently identified as RIG-I agonists, in particular *RNA5SP141* (Fig. 3A) (*12*).

To validate *RNA5SP141* as a transcriptional target of TFIIIA, we analyzed chromatin immunoprecipitation sequencing (ChIP-seq) data generated by the Encyclopedia of DNA Elements (ENCODE) consortium (Fig. 3C) (*29*). This analysis showed substantially more sequencing reads in the genomic region of *RNA5SP141* than in the input control, supporting that TFIIIA is a transcriptional regulator of *RNA5SP141* (Fig. 3C). *RNA5SP141* transcript levels were reduced in peripheral blood mononuclear cells (PBMCs) of unaffected carrier (II:3) and patient (II:2) as well as in TFIIIA C195W/C219R KI HEK293T cells or the respective mutant TFIIIA homozygous cell clones as compared with control cells (Fig. 3, D and E). In accord, silencing of *GTF3A* in primary normal human lung fibroblasts (NHLFs) and human alveolar epithelial cells (A549) also reduced *RNA5SP141* levels (Fig. 3F and fig. S4C).

Because TFIIIA and *RNA5SP141* are reportedly expressed in many different tissues and cell types (*12*, *30*), we asked whether TFIIIA regulates *RNA5SP141* biogenesis in neuronal cells, which are relevant target cells of HSV-1 infection. Silencing of TFIIIA in SH-SY5Y neuroblastoma cells markedly diminished *RNA5SP141* levels, indicating that neuronal cells also require TFIIIA for *RNA5SP141* transcription (fig. S4D).

To confirm that the identified *GTF3A* mutations impair *RNA5SP141* transcription in patient fibroblasts, we reconstituted these cells with WT TFIIIA and observed restored *RNA5SP141* expression (Fig. 3, G and H). In contrast, ectopic expression of the DNA binding–defective TFIIIA mutants with ZF3 or ZF7 deletion (ZF3KO and ZF7KO) failed to increase *RNA5SP141* expression (Fig. 3, I and J). These data indicate that LOF mutations in *GTF3A* lead to diminished transcription of the RIG-I ligand *RNA5SP141* at steady state.

Mutated *GTF3A* results in impaired *RNA5SP141* up-regulation during HSV-1 infection

RNA5SP141 is up-regulated during HSV-1 infection and relocalizes to the cytoplasm, where it binds to RIG-I (*12*). We observed impaired *RNA5SP141* up-regulation after HSV-1 infection in carrier and patient fibroblasts compared with a ~2-fold induction in infected HC cells (Fig. 4A). In contrast to *RNA5SP141*, TFIIIA expression remained unchanged by HSV-1 infection in fibroblast cells (fig. S5A). The abundance of the *RNA5SP141*-binding proteins TST and MRPL18, which prevent RIG-I activation in uninfected cells through *RNA5SP141* "masking" (*12*), was comparable in unaffected carrier, patient, and HC fibroblasts (fig. S5B). Moreover, we observed that *RNA5SP141* and RIG-I levels were up-regulated by HSV-1 infection also in neuroblastoma cells; in contrast, *GTF3A* mRNA and TFIIIA protein abundances were unchanged after HSV-1 infection (fig. S5, C and D).

Consistent with our results showing impaired *RNA5SP141* levels in HSV-1–infected patient fibroblasts, silencing of *GTF3A* in primary NHLFs also led to diminished up-regulation of *RNA5SP141* expression after HSV-1 infection (Fig. 4B).

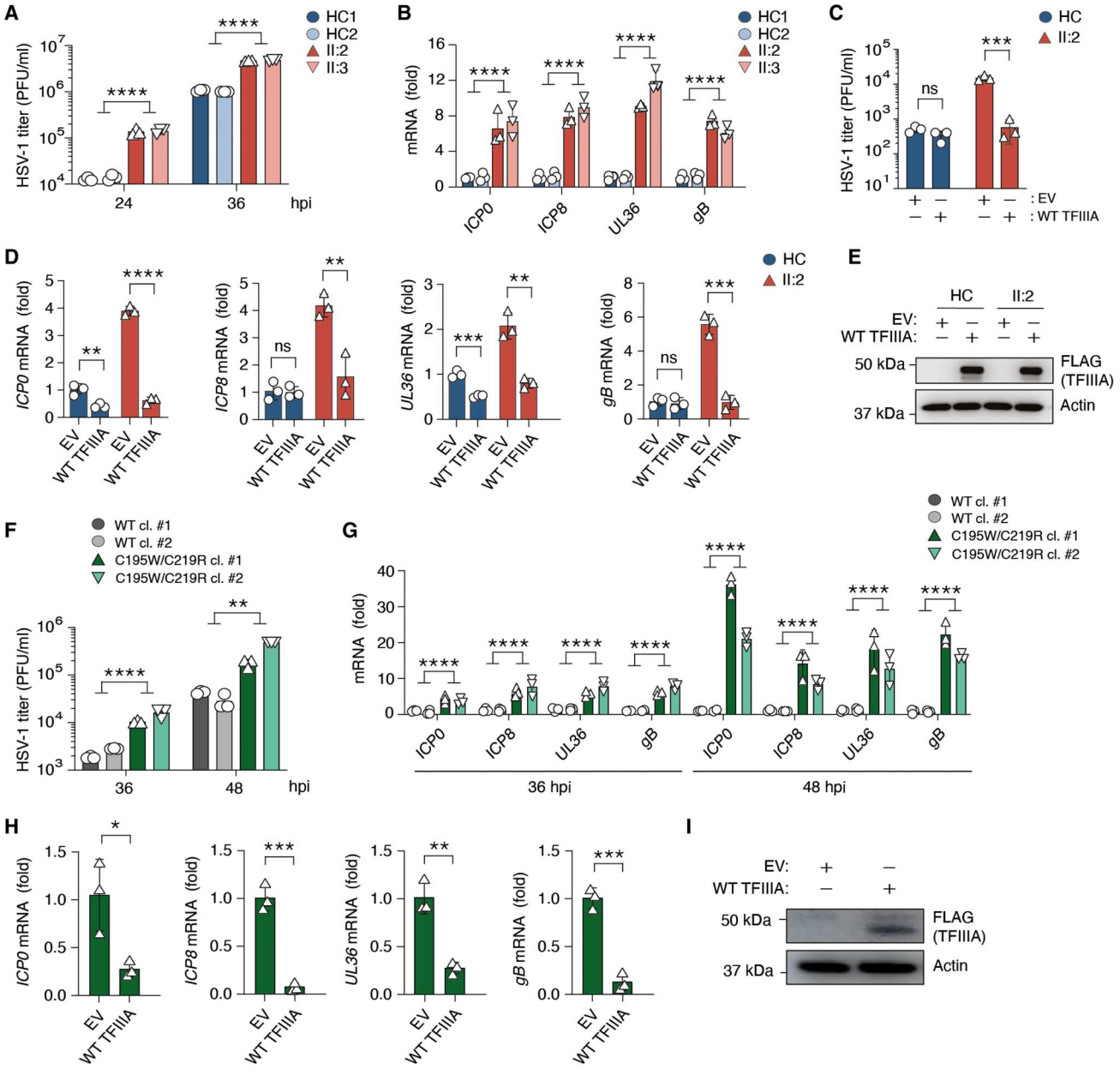

Fig. 2. Impaired cell-intrinsic defense to HSV-1 in *GTF3A* mutant cells. (**A**) Viral titers in the supernatant of fibroblasts from HCs, II:2, and II:3 that were infected with HSV-1 (MOI: 0.01) for the indicated times, determined by plaque assay. PFU, plaque-forming units; hpi, hours post-infection. (**B**) RT-qPCR of the indicated viral transcripts in fibroblasts from HCs, II:2, and II:3 infected with HSV-1 (MOI: 0.01) for 48 hours. (**C**) Viral titers in the supernatant of fibroblasts from HC and II:2 that were transfected for 30 hours with EV or FLAG-TFIIIA WT and then infected with HSV-1 (MOI: 0.02) for 48 hours. (**D**) RT-qPCR analysis of the indicated viral transcripts for the experiment in (C) relative to the values for EV-transfected HCs. (**E**) Representative expression of FLAG-TFIIIA for (C) and (D), determined by IB. (**F**) Viral titers in the supernatant of TFIIIA WT and C195W/C219R KI HEK293T clonal cell lines (clones #1 and #2) that were infected with HSV-1 (MOI: 0.01) as indicated, determined by plaque assay. (**G**) RT-qPCR of the indicated viral transcripts in TFIIIA WT and C195W/C219R KI HEK293T clonal cell lines that were infected as in (F). Values are presented relative to those from WT cells at each time point. (**H**) RT-qPCR analysis of the indicated viral transcripts in TFIIIA C195W/C219R KI HEK293T cells that were transfected for 30 hours with EV or FLAG-TFIIIA WT and then infected with HSV-1 (MOI: 0.02) for 48 hours. (**I**) Representative expression of FLAG-TFIIIA for (H), determined by IB. Data are representative of at least two independent experiments [mean ± SD of $n = 3$ biological replicates in (A) to (D) and (F) to (H)]. $^{*}P < 0.05$, $^{**}P < 0.01$, $^{***}P < 0.001$, $^{****}P < 0.0001$ (two-tailed, unpaired Student's t test).

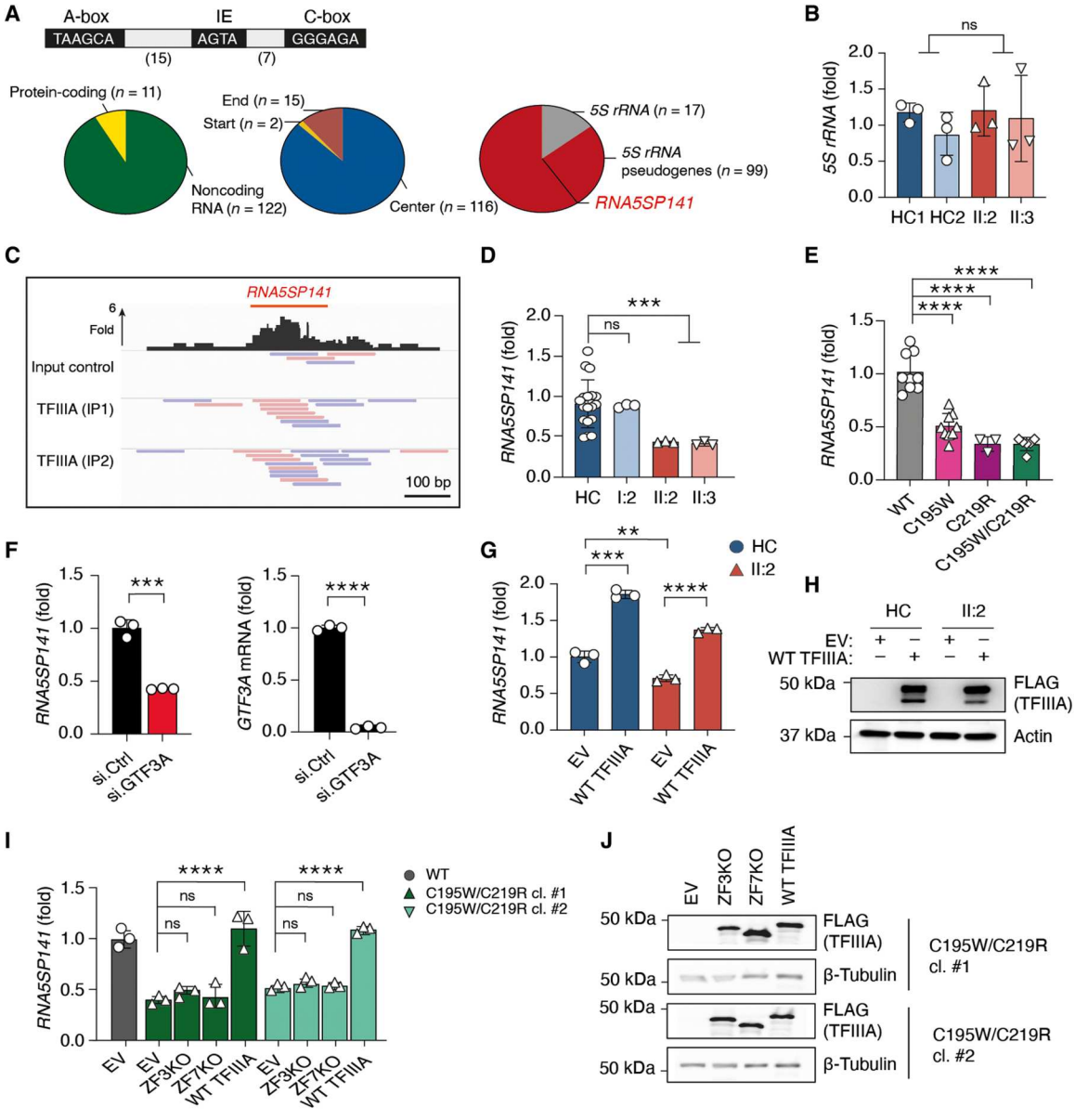

Fig. 3. The 5S rRNA pseudogene *RNA5SP141* is a transcriptional target of TFIIIA. (**A**) Genomic mapping of the ICR (top) using UROPA software (bottom panels). Genes with a centrally located ICR comprise parental *5S rRNA* transcripts and *5S rRNA* pseudogenes, including *RNA5SP141* (bottom right). (**B**) RT-qPCR analysis of *5S rRNA* in primary fibroblasts from II:2 and II:3 compared with HCs. (**C**) Sequencing reads at the *RNA5SP141* genomic locus, determined by ENCODE consortium ChIP-seq TFIIIA data analysis. IP1 and IP2 indicate two independent experiments. Data are presented as fold change relative to the values for input control. (**D**) RT-qPCR analysis of *RNA5SP141* in PBMCs from I:2, II:2, and II:3 compared with HCs ($n = 6$). (**E**) RT-qPCR analysis of *RNA5SP141* in TFIIIA WT ($n = 3$ clones) compared with TFIIIA C195W ($n = 3$ clones), C219R ($n = 1$ clone), and C195W/C219R ($n = 2$ clones) KI HEK293T cells. (**F**) Left: *RNA5SP141* levels in primary NHLFs that were transfected for 48 hours with either nontargeting control siRNA (si.Ctrl) or *GTF3A*-specific siRNA (si.GTF3A), determined by RT-qPCR. Right: *GTF3A* knockdown efficiency was confirmed by RT-qPCR. (**G**) RT-qPCR analysis of *RNA5SP141* expression in fibroblasts from HC and II:2 that were transfected for 48 hours with EV or FLAG-tagged WT TFIIIA. (**H**) Representative expression of FLAG-tagged WT TFIIIA for (G), determined by IB. (**I**) RT-qPCR analysis of *RNA5SP141* in TFIIIA WT and C195W/C219R KI HEK293T cells (clones #1 and #2) that were transfected for 24 hours with EV or FLAG-tagged TFIIIA WT or its mutants (ZF3KO and ZF7KO). (**J**) Expression of TFIIIA WT or mutants for (I), determined by IB. Each data point (B and E) represents one biological replicate from three independent experiments (mean ± SD), or data shown are representative of at least two (D and F to J) independent experiments [mean ± SD of at least $n = 3$ biological replicates in (D), (F), (G), and (I)]. $^{**}P < 0.01$, $^{***}P < 0.001$, $^{****}P < 0.0001$ [two-tailed, unpaired Student's *t* test (B, D, F, and G) or one-way ANOVA (E and I)].

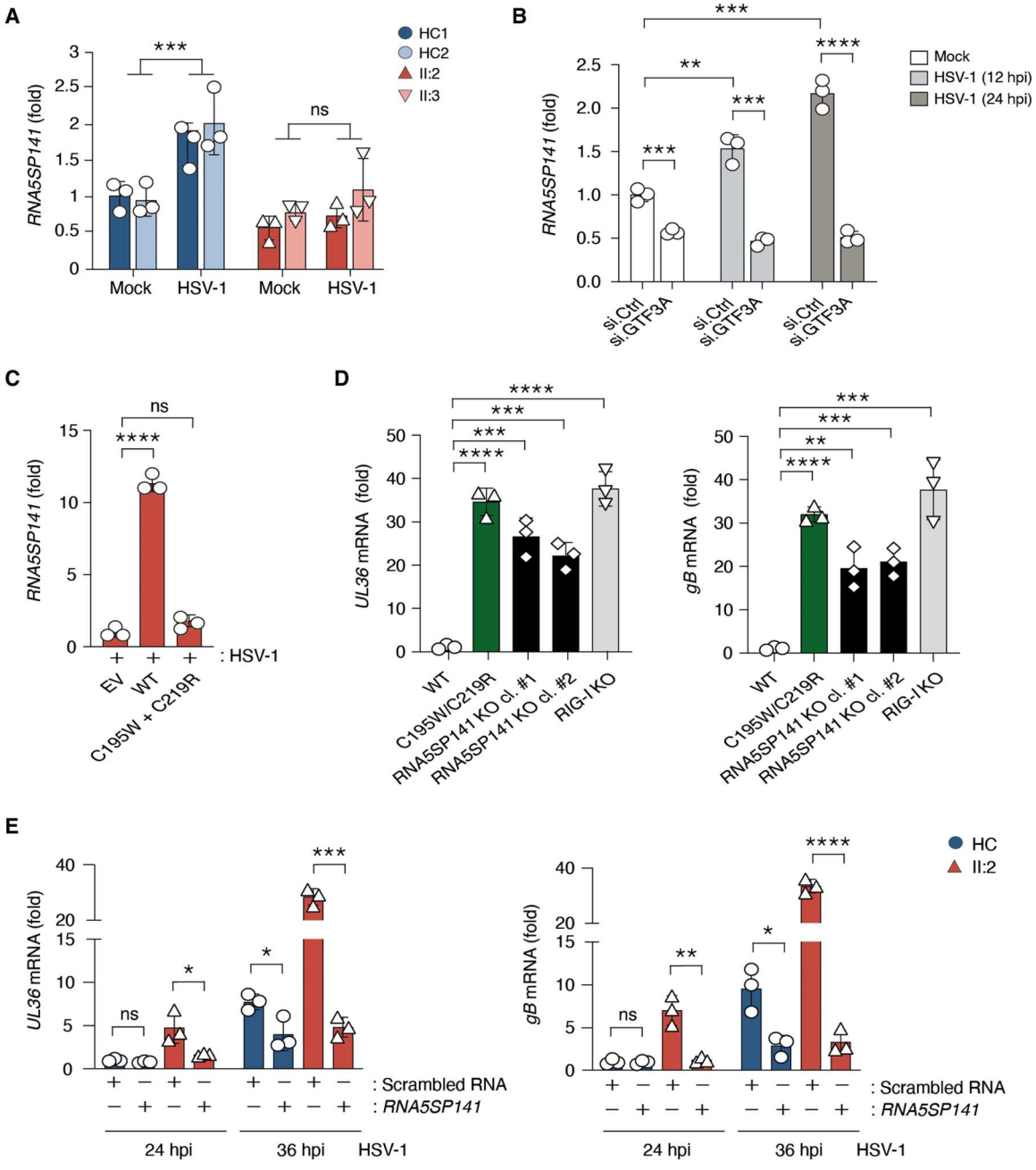

Fig. 4. *GTF3A* mutant cells have abrogated *RNA5SP141* up-regulation during HSV-1 infection, and exogenous *RNA5SP141* restores virus control. (**A**) RT-qPCR analysis of *RNA5SP141* transcripts in primary fibroblasts from II:2, II:3, and HCs that were either mock-treated or infected with HSV-1 (MOI: 1) for 24 hours. (**B**) RT-qPCR analysis of *RNA5SP141* in primary NHLF cells that were transfected for 48 hours with si.Ctrl or si.GTF3A, followed by either mock treatment or HSV-1 infection (MOI: 1) for the indicated times. (**C**) RT-qPCR analysis of *RNA5SP141* transcripts in fibroblasts from II:2 that were transfected for 30 hours with either EV or FLAG-tagged TFIIIA WT or the C195W and C219R mutants (1:1 ratio) and then infected with HSV-1 (MOI: 4) for 16 hours. (**D**) Viral transcripts in TFIIIA WT or C195W/C219R KI, *RNA5SP141* KO (clones #1 and #2), and *RIG-I* KO HEK293T cells that were infected with HSV-1 (MOI: 0.01) for 48 hours, determined by RT-qPCR analysis. (**E**) RT-qPCR analysis of the indicated viral transcripts in HC and II:2 fibroblasts that were infected as indicated with HSV-1 (MOI: 0.1) and, 4 hours later, transfected with either scrambled RNA (control) or IVT *RNA5SP141* (each 1 pmol). Data (A to E) are representative of at least two independent experiments (mean ± SD of $n = 3$ biological replicates). *$P < 0.05$, **$P < 0.01$, ***$P < 0.001$, ****$P < 0.0001$ (two-tailed, unpaired Student's t test).

Reconstitution of patient fibroblasts with WT TFIIIA, but not with the C195W and C219R TFIIIA mutants, markedly enhanced *RNA5SP141* expression upon HSV-1 infection (Fig. 4C and fig. S5E). Similar to TFIIIA C195W/C219R KI cells and *RIGI* KO cells, *RNA5SP141* KO HEK293T cells, with excision of this small noncoding RNA, exhibited increased HSV-1 gene expression compared with WT control cells (Fig. 4D and fig. S5F). *RNA5SP141* KO cells also supported higher HSV-1 titers than WT cells (fig. S5G). Inversely, transfection of patient fibroblasts with in vitro transcribed (IVT) *RNA5SP141* suppressed HSV-1 replication to comparable or lower levels as in nontransfected HC cells (Fig. 4E). These data indicate that TFIIIA transcriptionally up-regulates *RNA5SP141* during HSV-1 infection, which is important for virus control.

Impaired RIG-I activation after HSV-1 infection in *GTF3A* mutant cells

RNA5SP141 via its sensor RIG-I restricts HSV-1 infection through activation of IFN-I–mediated antiviral responses. We therefore examined the effect of exogenous IFN-I stimulation, or inversely IFN-α/β receptor 2 (IFNAR2)–blocking antibodies, on the HSV-1 phenotype observed for patient and HC fibroblasts. Stimulation of patient cells with IFN-α suppressed HSV-1 replication to comparable levels as those in untreated HC cells (fig. S6A). In contrast, anti-IFNAR2 treatment of HC cells robustly enhanced HSV-1 replication to levels even higher than those in untreated patient cells, suggesting a partial loss of intrinsic control of HSV-1 in the patient fibroblasts (fig. S6, B and C).

We investigated the direct impact of *GTF3A* mutations on RIG-I activation by examining its K63-linked ubiquitination and binding to the E3 ligase TRIM25, two key steps in RIG-I signal initiation (*31*). Co-immunoprecipitation (co-IP) studies showed that RIG-I exhibited abrogated K63-linked ubiquitination and a near-complete loss of TRIM25 binding in mutant *GTF3A* patient fibroblasts infected with HSV-1 (Fig. 5A). However, RIG-I ubiquitination and RIG-I–TRIM25 binding were comparable in patient and HC fibroblasts after transfection with IVT *RNA5SP141* or upon infection with Sendai virus (SeV), which is an RNA virus that activates RIG-I independently of *RNA5SP141* (Fig. 5, A and B) (*12*), ruling out that RIG-I activation is generally impaired in *GTF3A* mutant cells. Next, we monitored key signaling events downstream of RIG-I, specifically the phosphorylation of TANK-binding kinase 1 (TBK1), IFN regulatory factor 3 (IRF3), and signal transducer and activator of transcription 1 (STAT1). These proteins were expressed normally in *GTF3A* mutant fibroblasts (at comparable levels to those in HC cells) but showed markedly reduced phosphorylation upon HSV-1 infection, indicative of reduced activation (Fig. 5, C and D, and fig. S6D). In contrast, TBK1 and STAT1 phosphorylation was comparable in HC and patient fibroblasts upon infection with SeV or after transfection with IVT *RNA5SP141* or the rabies virus leader RNA [RABVle; a viral 5′-triphosphate RNA known to activate RIG-I (*12*)] (Fig. 5E and fig. S6E).

We compared HSV-1 transcripts in TFIIIA C195W/C219R KI and *RIGI* KO cells to those in cells deficient of the adaptor protein MAVS (*MAVS* KO) and found similarly increased HSV-1 replication (fig. S6, F and G). Moreover, whereas knockdown of endogenous *RIGI* or *MAVS* did not further enhance HSV-1 replication in the patient fibroblasts or in TFIIIA C195W/C219R KI cells, a significant increase in HSV-1 replication was observed upon *RIGI* or *MAVS* silencing in the respective control cells (Fig. 5, F and G, and fig. S6, H and I). Together, these data show abrogated *RNA5SP141*-induced RIG-I antiviral signaling in *GTF3A* mutant cells after HSV-1 infection.

Blunted IFN-I response in *GTF3A* mutant cells after HSV-1 infection

To evaluate the impact of impaired *RNA5SP141* biogenesis on antiherpesviral immunity, we examined the antiviral gene responses to HSV-1 infection. HSV-1–induced *IFNB1* and *IFIT1* transcripts were significantly lower in *GTF3A* mutant unaffected carrier and patient fibroblasts as compared with HC cells (Fig. 6, A and B, left panels). In contrast, the *GTF3A* mutant fibroblasts displayed normal innate immune responses to SeV (Fig. 6, A and B, right panels). Antiviral gene induction in the carrier and patient fibroblasts after extracellular polyinosinic:polycytidylic acid (poly(I:C)) stimulation was comparable to that in control cells (fig. S7, A and B), indicating that the *GTF3A* mutations do not affect TLR3 signaling. Furthermore, silencing of endogenous RIG-I, but not TLR3, abrogated antiviral gene expression in NHLF cells after IVT *RNA5SP141* transfection, ruling out a potential cross-talk between TLR3 and *RNA5SP141*-induced RIG-I signaling (fig. S7, C and D).

In line with the results in the patient fibroblasts, we found impaired antiviral cytokine responses to HSV-1 infection in TFIIIA C195W/C219R KI HEK293T cells as well as in the homozygous TFIIIA C195W and C219R cell clones (fig. S8, A and B). In accord, *RNA5SP141* KO HEK293T cells showed reduced antiviral gene induction after HSV-1, but not SeV, infection (fig. S8, C to F). *GTF3A* knockdown in primary NHLFs also diminished the induction of *IFNB1* and *IFIT1* mRNA during HSV-1 infection comparably to silencing of *RNA5SP141* or *RIGI* (Fig. 6, C and D, left panels, and fig. S8G). However, silencing of *GTF3A* or *RNA5SP141* did not, or only minimally, affect SeV-induced *IFNB1* and *IFIT1* expression, whereas knockdown of *RIGI* abrogated antiviral gene induction after SeV infection (Fig. 6, C and D, right panels, and fig. S8G).

RNA5SP141 also stimulates RIG-I–mediated cytokine responses to EBV and influenza A virus (IAV) infection (*12*), the latter being unique among RNA viruses due to its nuclear replication strategy. We therefore tested the effect of *GTF3A* silencing on EBV- and IAV-induced innate immune responses and found diminished cytokine/ISG transcripts upon *GTF3A* depletion, similarly to silencing of *RNA5SP141* or *RIGI* (fig. S9, A to H). Collectively, these results show that *GTF3A* deficiency abrogates expression of the endogenous RIG-I ligand *RNA5SP141*, which ultimately diminishes IFN-I and ISG responses to HSV-1 infection. Our data further suggest that TFIIIA, via *RNA5SP141* biogenesis, also regulates RIG-I–mediated innate immunity to EBV and IAV infection, although the physiological relevance of TFIIIA in intrinsic control of these two viruses warrants further investigation.

DISCUSSION

TFIIIA, encoded by *GTF3A*, has essential roles in ribosomal biogenesis by generating and stabilizing 5*S* rRNA. In this study, we identified compound heterozygous *GTF3A* mutations in a patient with CVID and afflicted by HSE in early childhood. Our work unveils TFIIIA acting as a moonlighting protein in anti–HSV-1 immunity

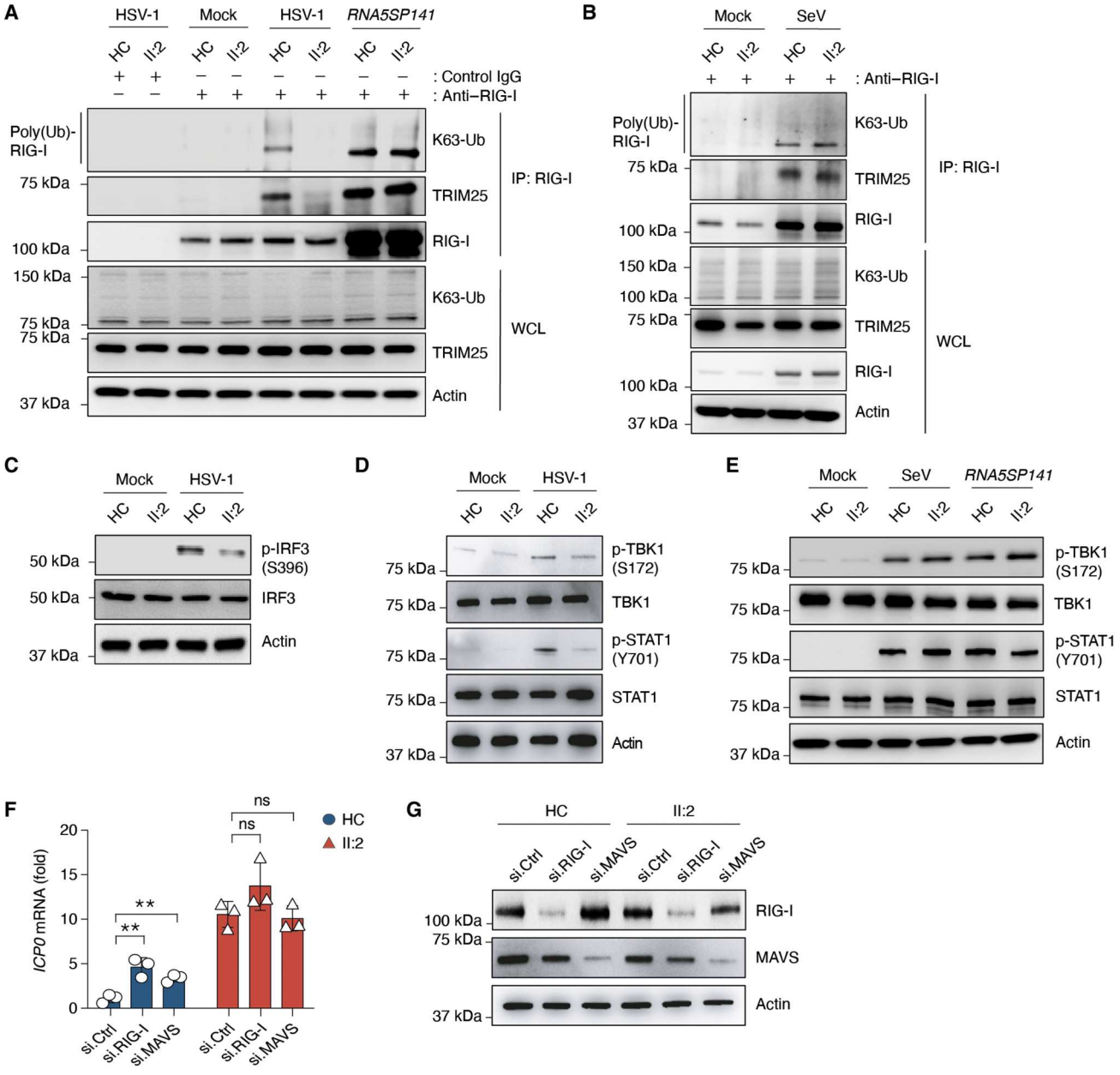

Fig. 5. Impaired RIG-I activation and downstream signaling in *GTF3A* mutant cells after HSV-1 infection. (**A**) K63-linked ubiquitination (Ub) of RIG-I and its binding to TRIM25 in HC and II:2 fibroblasts that were either mock-treated, infected with HSV-1 (MOI: 4), or transfected with IVT *RNA5SP141* (1 pmol) for 16 hours, determined by IP with anti–RIG-I. (**B**) K63-linked ubiquitination of RIG-I and its binding to TRIM25 in HC and II:2 fibroblasts that were either mock-treated or infected with SeV [5 HAU (hemagglutination units)/ml] for 16 hours, determined as in (A). (**C**) Phosphorylation of IRF3 (at S396) in HC and II:2 fibroblasts that were either mock-treated or infected with HSV-1 (MOI: 4) for 16 hours, determined in the WCLs by IB. (**D**) Phosphorylation of TBK1 (at S172) and STAT1 (at Y701) in HC and II:2 fibroblasts that were either mock-treated or infected with HSV-1 (MOI: 4) for 16 hours, determined in the WCLs by IB. (**E**) Phosphorylation of TBK1 (at S172) and STAT1 (at Y701) in HC and II:2 fibroblasts that were either mock-treated, infected with SeV (5 HAU/ml), or transfected with IVT *RNA5SP141* (1 pmol) for 16 hours, determined as in (D). (**F**) RT-qPCR analysis of HSV-1 *ICP0* transcripts in HC and II:2 fibroblasts that were transfected for 30 hours with si.Ctrl, si.RIG-I, or si.MAVS and then infected with HSV-1 (MOI: 0.01) for 36 hours. (**G**) Knockdown efficiency of RIG-I and MAVS for (F) was determined by IB. Data are representative of at least two independent experiments [mean ± SD of $n = 3$ biological replicates in (F)]. $^{**}P < 0.01$ (two-tailed, unpaired Student's *t* test).

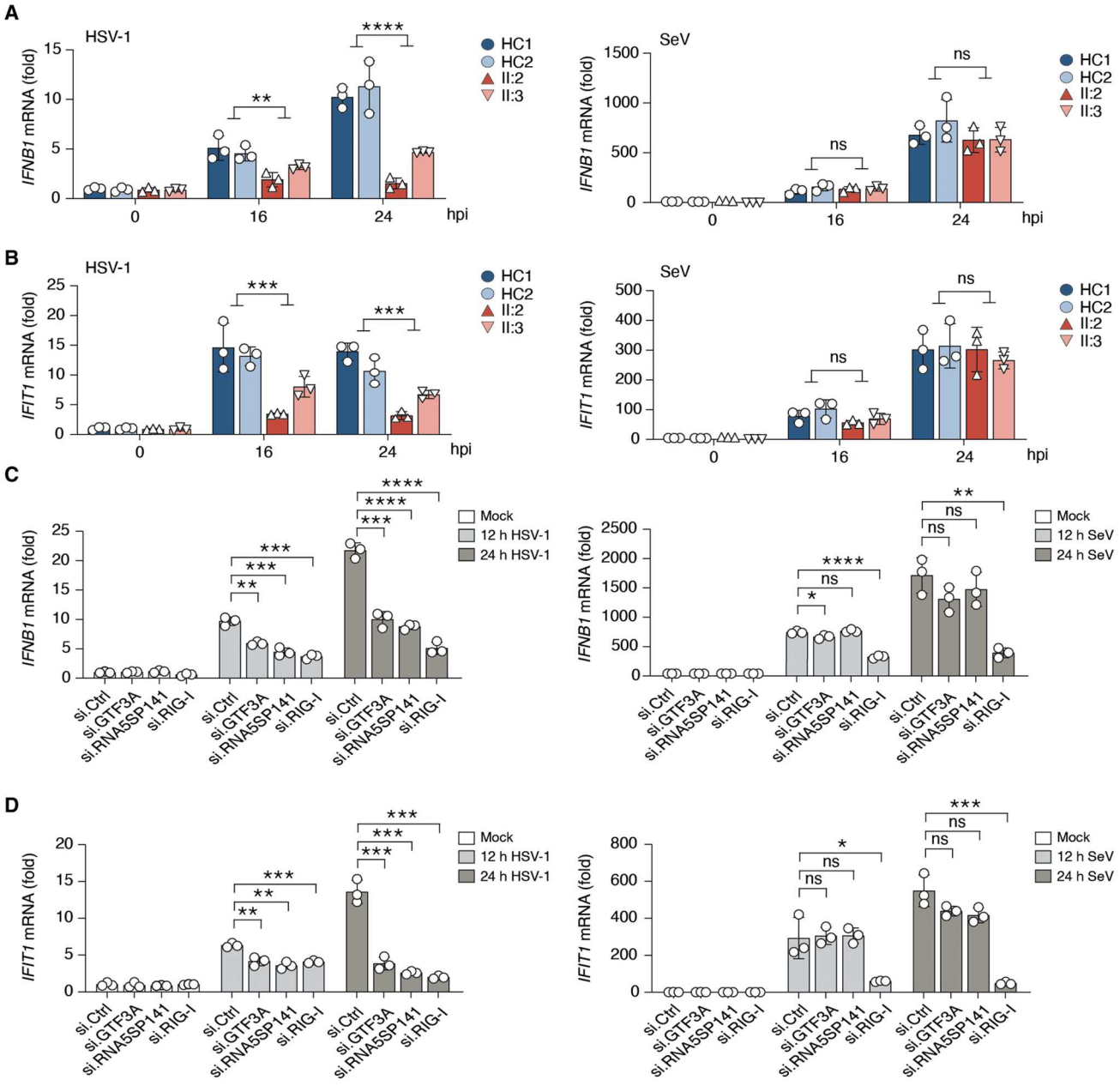

Fig. 6. Antiviral innate immune responses are blunted in HSV-1–infected *GTF3A* mutant cells. (**A**) RT-qPCR analysis of *IFNB1* transcripts in primary fibroblasts from II:2, II:3, and HCs that were infected with either HSV-1 (MOI: 1) (left) or SeV (10 HAU/ml) (right) for the indicated times. (**B**) RT-qPCR analysis of *IFIT1* transcripts in primary fibroblasts from II:2, II:3, and HCs that were infected as in (A). (**C**) RT-qPCR analysis of *IFNB1* transcripts in primary NHLF cells that were transfected for 48 hours with the indicated siRNAs and then either mock-treated or infected with HSV-1 (MOI: 1) (left) or SeV (10 HAU/ml) (right) for the indicated times. (**D**) RT-qPCR analysis of *IFIT1* transcripts in primary NHLF cells that were transfected and infected as in (C). Data are representative of at least two independent experiments (mean ± SD of $n = 3$ biological replicates). *$P < 0.05$, **$P < 0.01$, ***$P < 0.001$, ****$P < 0.0001$ (two-tailed, unpaired Student's t test).

by generating *RNA5SP141*, an endogenous ligand of the RNA sensor RIG-I.

The mutations in *GTF3A* target Cys residues that are essential for the stabilization of the ZF structure (*32*). The TFIIIA C195W mutant represents a hypomorphic variant and shows reduced (but not abolished) interaction with the 5*S* rDNA ICR and preserved 5*S* rRNA transcription, whereas TFIIIA C219R shows severely impaired DNA binding affinity. The combination of a null mutation and a variant with residual activity might be key to the observed phenotype. Whereas biallelic *GTF3A* null variants may result in embryonic lethality, biallelic hypomorphic variants of TFIIIA may cause a different clinical spectrum. gnomAD does not annotate healthy individuals harboring homozygous truncating *GTF3A* mutations (*26*). A similar inheritance pattern has been observed for other genetic diseases with biallelic mutations targeting essential housekeeping genes (*33*–*35*).

The proband developed HSE, whereas his sibling carrying the same biallelic mutations did not. Nonetheless, our data revealed an intrinsic defect in innate antiviral defense against HSV-1 in fibroblasts of both siblings. This incomplete clinical penetrance has also been reported for other genetic defects causing HSE. For example, monogenic errors of the TLR/IFN-I pathway cause sporadic, but not familial, occurrence of HSE (*2*, *16*). (Epi)genetic modifiers, viral inoculum or strain, and environmental factors may play a role in determining the degree of clinical penetrance.

We here identify the RIG-I ligand *RNA5SP141* as a bona fide transcriptional target of TFIIIA (*12*). During HSV-1 infection, this small noncoding RNA is relocated from the nucleus to the cytoplasm and is unmasked through down-regulation of the *RNA5SP141*-binding proteins TST and MRPL18 (*12*). This allows *RNA5SP141* to bind RIG-I and induce IFN-I responses, which exhibit delayed kinetics as compared with those induced by DNA sensors (i.e., cGAS) that sense HSV-1 immediately after infection (*12*). Our work showed that *GTF3A* mutant cells have impaired *RNA5SP141* expression during HSV-1 infection, resulting in blunted RIG-I activation and IFN-I responses. Although most of our experiments were performed in primary fibroblasts and epithelial cell lines, our data in neuroblastoma cells suggest that neurons similarly require TFIIIA for *RNA5SP141* transcription. However, future studies determining the relevance of the TFIIIA–*RNA5-SP141*–RIG-I axis in HSV-1 restriction in neurons are required to confirm a causal relationship between *GTF3A* mutations and HSE, as outlined by key criteria for single-patient genetic studies (*36*). Our work also suggests that TFIIIA, via *RNA5SP141* (*12*), mediates innate immunity to EBV and IAV. To date, however, no severe clinical infections with EBV or IAV have been documented in either patient.

A growing body of literature documents the role of RIG-I–like receptor (RLR)–mediated sensing of endogenous ligands in autoimmune diseases and cancer (*8*, *37*). Similar to *RNA5SP141*, the host-derived RLR ligands found in these disease contexts are typically noncoding RNAs, however, from different subclasses (*38*–*40*). RNA mislocalization, changes in the stoichiometry of RNA versus RNA-binding proteins, and impairment of specific RNA-modifying enzymes (e.g., DUSP11 and ADAR1) have been found to underlie aberrant RLR activation (*38*, *40*–*43*). Our work shows that host-derived RIG-I agonists serve as damage-associated molecular patterns (DAMPs) mediating "indirect" sensing of virus infection, much akin to the guard hypothesis in plant immunity (*44*), and that defective production of these endogenous ligands can cause viral disease in humans.

Most characterized RIG-I agonists contain a 5′ triphosphate group (*8*), a feature that is found in viral RNA molecules but absent in the vast majority of host cytosolic RNAs (*8*). As an exception, Pol III transcribes small 5′ triphosphate RNAs from host DNA, which requires TFIIIA as well as TFIIIC and TFIIIB (*17*). Our results identified that TFIIIA mediates Pol III–dependent *RNA5SP141* transcription, which restricts HSV-1 infection. Inborn errors in Pol III subunits have been associated with severe VZV infections (*45*, *46*). Whether impaired *RNA5SP141* expression in individuals with germline Pol III mutations contributes to enhanced susceptibility to VZV infection remains to be determined.

TFIIIA is widely expressed across tissues; therefore, the clinical spectrum of *GTF3A* mutations could extend beyond impaired innate antiviral responses. Both siblings harboring *GTF3A* mutations display a CVID-like phenotype, resulting in susceptibility to bacterial respiratory infections during childhood and poor pneumococcal antibody responses, but they exhibit differences in B cell maturation defects and Ig levels. At present, both siblings are in good clinical condition without Ig replacement treatment, reflecting a mild antibody deficiency. Only a few monogenic defects underlie CVID, which is mainly defined as a polygenic, multifactorial disease (*47*). Future research including studies in mice is required to investigate a potential causal role of *GTF3A* mutations in the dysfunction of other immune system components and the other clinical presentations observed. In line with this notion, recent work on TRAF3 deficiency, initially described as a genetic etiology of HSE (*48*), has now been associated with B cell dysfunction in patients exhibiting an immune dysregulation syndrome (*49*).

In conclusion, our study reveals TFIIIA as a moonlighting protein that not only mediates 5*S* rRNA transcription but also regulates innate immune responses to HSV-1 by transcribing the host-derived RIG-I ligand *RNA5SP141*. We further show that *GTF3A* mutations in humans confer impaired cell-intrinsic anti–HSV-1 immunity and are associated with HSE, expanding the genetic etiology and immunological mechanisms of invasive herpesviral disease.

MATERIALS AND METHODS

Study approval

This study was approved by the ethics committee of the Ghent University Hospital in Belgium (2012/593). Demographic and clinical data on the participating individuals were registered in an in-house stored, protected, and anonymized data file. Clinical information and samples were obtained with informed consent from the participants of the study, in accordance with the 1975 Helsinki Declaration.

Sequencing

WES of index and unaffected parents was performed on gDNA using a SureSelect Human All Exon V5 kit (Agilent) or Twist Human Core Exome enrichment with additional probes for humane RefSeq transcripts (Twist Bioscience). Paired-end massively parallel sequencing (2 × 150 cycles) was performed on NovaSeq 6000 (Illumina). Data analysis was accomplished with an in-house developed pipeline, in accordance with international guidelines. Consensus *SNORA31* sequence (NR_002967) was analyzed and identified by Sanger sequencing. Sequence validation and segregation analysis of the candidate variants in *GTF3A* (NM_002097.3) were performed with Sanger sequencing.

Protein modeling of TFIIIA

The model of the three-dimensional (3D) protein structure of WT human TFIIIA (UniProtKB ID Q92664) was predicted using AlphaFold Database (*50*, *51*). Structure images and protein mutagenesis (C195W, C219R, and R89C) were created in PyMOL.

Immunophenotyping

Cryopreserved human PBMCs were thawed using complete medium (RPMI 1640 medium) supplemented with GlutaMAX, 10% fetal calf serum (FCS; Sigma-Aldrich), 1% penicillin-streptomycin (10,000 U/ml; Gibco, 15140122), 1 mM sodium pyruvate (Gibco, 11360070), 1% nonessential amino acids (NEAAs; Gibco,

11140035), and 50 μM 2-mercaptoethanol (Gibco, 31350010). After centrifugation (400*g* for 7 min) and removal of supernatant, cells were resuspended and left to recuperate for 30 min. About 5 million cells per sample were stained (based on counts before cryopreservation). Cells were incubated with a fixable viability dye eFluor 780 (Thermo Fisher Scientific, 65-0865-14) for 20 min at 4°C and subsequently stained with fluorochrome-labeled antibodies (table S4) for 30 min at 4°C. Cells were fixed and permeabilized using the eBioscience Human Intracellular Protein Flow Cytometry Kit (Thermo Fisher Scientific, A53016) according to the manufacturer's protocol. To bind intracellular epitopes, antibodies were resuspended in permeabilization buffer and incubated with cell suspension for 30 min at room temperature. All patient and control samples were analyzed together. Acquisition of labeled cell suspensions was performed with a BD FACSymphony flow cytometer (BD Biosciences) and subsequent analysis was performed with FlowJo v10.7 (BD Biosciences).

Plasmids and cloning

The cDNA sequence encoding WT TFIIIA was inserted into a modified pcDNA3.1+ expression plasmid encoding a C-terminal 3xFLAG-tag or N-terminal GFP-tag and purchased from GenScript. All plasmids were propagated in DH5α *Escherichia coli* and isolated using NucleoSpin Plasmid EasyPure (Macherey-Nagel). For generating TFIIIA mutants, the respective mutations were introduced using the QuikChange Site-Directed Mutagenesis protocol according to the manufacturer's instructions (Agilent Technologies, #200518). To generate the C-terminal 3xFLAG-tagged TFIIIA ZF3KO and ZF7KO mutants and N-terminal GFP-tagged TFIIIA ZF7KO mutant, we used the LFEAP (Ligation of Fragment End After PCR) method as described previously (*52*).

Confocal microscopy imaging

HEK293T cells were reverse-transfected in eight-well chamber slides (~80,000 cells per well; Ibidi) with 200 ng of expression plasmids encoding GFP-TFIIIA WT, C195W, or C219R using Lipofectamine 2000 (Invitrogen, 11668-027). Twenty-four hours later, cells were fixed with 4% paraformaldehyde [in phosphate-buffered saline (PBS)] for 20 min, washed with PBS, and subsequently permeabilized using 0.5% Triton X-100 (in PBS) for 30 min. Cells were stained for 1 hour at room temperature with Alexa Fluor 633 phalloidin (1:100; Invitrogen, A22284) and Hoechst 33342 (1:1000; Invitrogen, H21492) in staining buffer (0.1% Triton X-100 in PBS), then washed in PBS and stored at 4°C until imaging. Confocal images were captured with a Zeiss LSM880 Airyscan confocal microscope using a 63× Plan-Apo/1.4 oil objective. *Z* stacks were taken with an interval of 0.16 μm in Fast Airyscan mode with a zoom of 1.8. Images were processed using Zen Black software and further analyzed using Fiji. Parameters such as detector gain, laser intensity, exposure time, and image postprocessing were kept consistent between the different conditions.

Image stream

HEK293T cells were seeded into 60-mm dishes containing ~1.4 million cells and reverse-transfected with the indicated plasmids for 24 hours. Cells were detached using 0.25% trypsin/0.04% EDTA (1:5 mixture) and washed with PBS. Next, cells were stained with a live/dead stain (eBioscience Fixable Viability Dye eFluor 780, Thermo Fisher Scientific, 65-0865-14) for 30 min at 4°C. Samples were washed in PBS and fixed using the eBioscience Foxp3/Transcription Factor Staining Buffer Set (Thermo Fisher Scientific, 00-5523-00). To visualize the nuclei, we incubated the cells in permeabilization buffer with 4′,6-diamidino-2-phenylindole (DAPI) (1:1000; Thermo Fisher Scientific, D21490) for 30 min at 4°C. Cells were washed twice and then resuspended in 50 μl of PBS and stored at 4°C until flow cytometric analysis (Amnis ImagestreamX MkII; Inspire). Processing of data was done using the IDEAS 6.3 software.

Electrophoretic mobility shift assay

HEK293T cells were seeded into six-well plates containing ~750,000 cells per well and reverse-transfected with the specified pcDNA3.1 expression vectors using Lipofectamine 2000 (Thermo Fisher Scientific, 11668-027). Sixteen hours later, cells were washed with ice-cold PBS and then lysed in radioimmunoprecipitation assay (RIPA) buffer [50 mM Tris-HCl (pH 7.5), 1% Igepal CA-630, 0.1% SDS, 0.5% deoxycholate, 150 mM NaCl, and cOmplete protease inhibitor cocktail (Merck, 11836170001)]. Ten micrograms of protein lysate were incubated with an IRDye 700–labeled 5*S* rRNA oligonucleotide (5′-AAGCTAAGCAGGGTCGGGCCTGGTTAGTACTTGGATGGGAGACCGC-3′) in 10× binding buffer [100 mM Tris, 500 mM KCl, and 10 mM dithiothreitol (DTT; pH 7.5)], 25 mM DTT/2.5% Tween 20, and poly(I:C) (1 μg/ml). After 30 min of incubation at room temperature, 10× Orange Loading Dye was added. Samples were loaded onto a 6% polyacrylamide gel, followed by electrophoresis (Mini-PROTEAN, Bio-Rad) at 100 V for 90 min. The signal was detected and quantified with an Odyssey infrared imaging system (LI-COR). Equal input for TFIIIA WT and mutants was confirmed by Western blot analysis.

Primary cell isolation

Primary human fibroblasts were isolated from a 5-mm skin punch biopsy. Epidermis was separated from dermis by scraping, and afterward, cells were isolated by incubation at 37°C with collagenase type II (Thermo Fisher Scientific) for at least 4 hours on a spinning rotor. Cells were stored in 90% FCS (Sigma-Aldrich) containing 10% dimethyl sulfoxide (DMSO; Sigma-Aldrich, D2650) at −150°C until further use. Peripheral venous blood specimens were collected from age-matched healthy individuals and patients using EDTA tubes. EDTA blood was diluted 1:2 in Hanks' balanced salt solution (Fisher Scientific, 24020117), and PBMCs were isolated after gradient centrifugation over Ficoll-Paque (GE Healthcare, 17-1440-02). PBMCs were aliquoted in culture medium and 10% DMSO. Vials were placed in a −80°C freezer using controlled rate freezing in preparation for final storage at −150°C until further use.

Cell culture

HEK293T cells [the American Type Culture Collection (ATCC)], A549 cells (ATCC), Vero cells (ATCC), NHLF (Lonza), SH-SY5Y (ATCC), and primary human fibroblast cells were maintained in Dulbecco's modified Eagle's medium (DMEM) supplemented with 10% FCS (Sigma-Aldrich) or fetal bovine serum (FBS; Gibco), 1% penicillin-streptomycin (10,000 U/ml; Gibco, 15140122), 200 mM L-glutamine (Gibco), 1 mM sodium pyruvate, and 50 mM 2-mercaptoethanol (Gibco) at 37°C and 5% CO_2. PBMCs were cultured in RPMI 1640 medium supplemented with GlutaMAX, 10% FCS, 1% penicillin-streptomycin (10,000 U/ml;

Gibco, 15140122), 1 mM sodium pyruvate (Gibco, 11360070), 1% NEAA (Gibco, 11140035), and 50 μM 2-mercaptoethanol (Gibco, 31350010). AGS-EBV cells (provided by N. Raab-Traub, UNC-Chapel Hill) were cultured in Ham's F12 supplemented with 10% FBS, 2 mM GlutaMAX (Gibco), 1% penicillin-streptomycin (10,000 U/ml), and G418 (500 μg/ml; Gibco). *RIGI* and *MAVS* KO HEK293T cells were generated by CRISPR-Cas9–mediated genome editing using guide RNAs (gRNAs) 5′-GGGTCTTCCGGATATAATCC-3′ and 5′-GGCCACCATCTG-GATTCCTT-3′, respectively. *RNA5SP141* KO HEK293T cells were generated by transient transfection of a plasmid vector containing single-guide RNA (sgRNA) 5′-GAAATACATC-CAAAAGTCTA-3′ and 5′-GATGATTAGAGGCTGTGTCTT-3′ together with an *RNA5SP141* homologous linearized repair plasmid with a Zeocin-resistant gene as selection marker. *RIGI* and *MAVS* KO cell lines were validated using immunoblotting (IB), and *RNA5SP141* KO cells were validated by Sanger sequencing and RT-qPCR analysis. Commercially obtained cells/cell lines were authenticated by the respective vendors and were not validated further in our laboratory. Cell lines that were obtained and validated by other groups were not further authenticated. All cell lines have been regularly tested for potential mycoplasma contamination by PCR.

Virus infection studies

Cells were infected with HSV-1 KOS strain (provided by D. Knipe, Harvard) or F strain (provided by W. J. Kaiser, Emory University; used in fig. S8, A and B) at the indicated multiplicity of infection (MOI). Briefly, infection of cells with HSV-1 was carried out in DMEM supplemented with 1% FBS, 2 mM glutamine, and 1% penicillin-streptomycin for 2 hours at 37°C. At the indicated times after infection, cells were lysed for RNA isolation and qPCR analysis of viral gene expression, or cell culture supernatants were harvested for viral titer analysis by standard plaque assay on Vero cells. SeV (Cantell strain) was purchased from Charles River Laboratories and used for cell infection as indicated. Reactivation of EBV in latently infected AGS-EBV cells (Akata strain) was induced by treatment with 2.5 mM sodium butyrate (Merck) dissolved in sterile water. Influenza A/Puerto Rico/8/1934(H1N1) WT and ΔNS1 recombinant virus were provided by A. García-Sastre (Mount Sinai).

Generation of TFIIIA mutant HEK293T clonal cell lines

Cells were electroporated (NEPA21, Nepagene) with the indicated gRNAs and GFP-tagged Cas9 (VIB Protein Service Facility). Homozygous TFIIIA C195W and TFIIIAC219R clones were generated by CRISPR-Cas9–mediated homology-directed repair and using gRNA#1 (5′-CGTCCATGTTTTTGCCACAA-3′) and gRNA#2 (5′-AAATACTATGTGAAGTATGC-3′), respectively. A single-stranded DNA (ssDNA) repair template oligo containing the C195W or C219R mutation was electroporated together with the Cas9/gRNA complex. Twenty-four hours after electroporation, single GFP-positive cells were fluorescence-activated cell sorting (FACS)–sorted and plated into 96-well plates. Clones were screened by PCR. C195W or C219R mutation in HEK293T clones was confirmed by Sanger sequencing, and subcloning of the PCR fragments was performed with the Zero Blunt TOPO PCR Cloning Kit (Thermo Fisher Scientific, 450245). At least 11 subclones were individually sequenced. One homozygous TFIIIA C219R clone was obtained by retargeting a TFIIIA WT/C219R clone using gRNA#3 (5′-ACTTCACGTAGTATTTCCTC-3′) and a corresponding ssDNA repair template oligo. TFIIIA C195W/C219R HEK293T clones were generated by additional CRISPR-Cas9–mediated homology-directed repair of a TFIIIA WT/C219R clone using gRNA#1 and an ssDNA repair template oligo containing the C195W mutation. TFIIIA C195W/C219R HEK293T clones were screened for the absence of WT allele by Sanger sequencing and subcloning of the PCR fragments.

Coimmunoprecipitation

Transfected and/or infected cells were harvested and lysed in 1 ml of NP-40 lysis buffer [50 mM Hepes (pH 7.4), 150 mM NaCl, and 1% NP-40] supplemented with protease inhibitor cocktail (MilliporeSigma, P2714) and phosphatase inhibitor cocktail (MilliporeSigma, P0044). One hundred microliters of the cell lysate was mixed with Laemmli loading buffer and used for whole-cell lysate (WCL) analysis. The remaining amount of cell lysate was incubated at 4°C overnight with about 1 to 2 μg of primary antibody or isotype-matched IgG antibody (control), followed by incubation with protein G Dynabeads (Invitrogen) for 2 hours at 4°C. IP or co-IP samples were washed rigorously with NP-40 lysis buffer and then analyzed by IB as described previously (*53*).

Immunoblotting

Proteins were resolved by Bis-Tris SDS–polyacrylamide gel electrophoresis and then transferred onto polyvinylidene difluoride membranes using wet or semidry IB. Membranes were blocked with 5% nonfat dry milk or bovine serum albumin (BSA) in TBS-T (Tris-buffered saline–0.1% Tween 20) typically for 1 hour and then probed with primary antibody in 5% nonfat dry milk or BSA (in TBS-T) at the indicated dilutions (as described below) overnight at 4°C. Membranes were washed in TBS-T and probed with horseradish peroxidase (HRP)–linked anti-mouse or anti-rabbit antibody in 5% nonfat dry milk or BSA (in TBS-T) for 1 hour at room temperature. Proteins were visualized using an enhanced chemiluminescence (ECL) reagent (Western Lightning Plus-ECL, PerkinElmer) or the SuperSignal West Pico PLUS or Femto chemiluminescence reagents (Thermo Fisher Scientific) on Amersham Imager 600 (General Electric) or ImageQuant LAS 4000 Chemiluminescent Image Analyzer (General Electric) as previously described (*53*). Primary and secondary antibodies for Western blotting are listed below.

Antibodies and other reagents

The antibodies (at the indicated dilutions) used for immunoblot analysis are the following: anti-TFIIIA (1:1000; Abcam, ab129440), anti–β-tubulin–HRP (1:2000; Abcam, ab21058), anti-GFP [Cell Signaling Technology (CST), monoclonal antibody #2956], anti-FLAG (1:2000; Sigma-Aldrich, M2), anti–RIG-I (1:2000; AdipoGen, Alme-1), anti-K63 linkage-specific polyubiquitin (1:1000; CST, D7A11), anti-TRIM25 (1:1000; BD Biosciences, 2/EFP), anti–phospho-IRF3 (S^{396}) (1:1000; CST, D6O1M), anti-IRF3 (1:1000; CST, D6I4C), anti–phospho-TBK1 (S^{172}) (1:1000; CST, D52C2), anti-TBK1 (1:1000; CST, D1B4), anti–phospho-STAT1 (Y^{701}) (1:1000; CST, 9167S), anti-STAT1 (1:1000; CST, 9172S), anti-RPL5 (1:1000; GeneTex, GTX101821), anti-TST antibody (1:1000; Abcam, ab166625), anti-MRPL18 (1:1000; Abcam, ab67844), anti-MAVS (1:1000; CST, 3993S), anti-TLR3 (1:1000; CST, D10F10), and anti-actin (1:5000; Sigma-Aldrich, A1978).

Secondary HRP-conjugated anti-mouse and anti-rabbit antibodies were used at a 1:5000 dilution and purchased from CST (catalog nos. 7076 and 7074, respectively) or Amersham (NA931 and NA934, respectively). Monoclonal anti-IFNAR2 antibody (clone MMHAR-2) and human IFN-α hybrid protein (universal type I IFN) were obtained from PBL Assay Science. Human IL-8/CXCL8 enzyme-linked immunosorbent assay (ELISA) (Bio-Techne, R&D Systems) was performed according to the manufacturer's instructions. High–molecular weight poly(I:C) was purchased from InvivoGen and used according to the manufacturer's instructions.

siRNA-mediated knockdown

Transient knockdown of endogenous *TFIIIA/GTF3A*, *RIGI/DDX58*, *MAVS*, and *TLR3* was achieved by transfection of gene-specific small interfering RNA (siRNA) targeting TFIIIA (Dharmacon, siGENOME SMARTpool, M-012635-01-0005), RIG-I (Dharmacon, siGENOME SMARTpool, M-012511-01-0010), MAVS (Dharmacon, M-024237-02-0005), or TLR3 (Dharmacon, M-007745-00-0020) using RNAiMAX transfection reagent (Invitrogen) according to the manufacturer's instructions. As a control, nontargeting siRNA (Dharmacon, D-001206-14-20) was transfected. Transient knockdown of endogenous *RNA5SP141* was achieved by RNAiMAX transfection of custom-made siRNA with the sense sequence 5′-UGGGAGAAAUACAUCCAAAUU-3′ (Dharmacon). Knockdown efficiency was confirmed by analyzing the transcript levels of the respective gene by RT-qPCR using specific primers [from Integrated DNA Technologies (IDT)] or by determining their protein abundance by immunoblot analysis.

RNA isolation and RT-qPCR analysis

Cells were lysed in RLT Plus buffer (QIAGEN) and stored at −80°C until further processing. RNA was isolated using the RNeasy Kit (QIAGEN) following the manufacturer's instructions. Concentration and purity of RNA was assessed using the NanoDrop 2000 technology. Equal amounts of RNA were transcribed to cDNA using the SensiFast cDNA Synthesis Kit (Bioline, BIO-65054). About 15 ng of cDNA was used as input for quantitative real-time PCR (Roche, LightCycler 480). cDNA values were normalized to respective *GAPDH* values. For the experiments that analyzed HSV-1 transcripts or cellular cytokines, total RNA was purified from cells using an RNA extraction kit (Omega Bio-Tek) according to the manufacturer's instructions. Equal amounts of RNA were used for a One-Step RT-qPCR reaction using the SuperScript III Platinum One-Step RT-qPCR kit with ROX (Life Technologies) on a 7500 Fast Real-Time PCR machine (Applied Biosystems). Relative quantitation of target cDNA was determined by the formula $2^{-\Delta\Delta Ct}$, with ΔΔCt denoting fold increases above the respective controls and values normalized to *GAPDH*. For EBV *BMRF1* transcript analysis, custom FAM reporter dye primers were used (forward, 5′-CAACACCGCACTGGAGAG-3′; reverse, 5′-GCCTGCTTCACTTTCTTGG-3′; probe, 5′-AGGAAAAGGACATCGTCGGAGGC-3′) (IDT). For *RNA5SP141* transcript analysis, total RNA including all small RNAs was isolated from cells using either the mirVana microRNA Isolation Kit (Life Technologies) or Quick-RNA Miniprep Kit (Zymo Research). RT reactions were carried out by using *RNA5SP141*- and *Let-7a*–specific TaqMan MicroRNA Assay primers, followed by RT-qPCR analysis using *RNA5SP141*-specific (Thermo Fisher Scientific, catalog no. CSN1ESE) and *Let-7a*–specific (Thermo Fisher Scientific, catalog no. 4440887) TaqMan FAM reporter dye probes and TaqMan Fast Advanced Master Mix. Fold expression levels of *RNA5SP141* were normalized to *Let-7a* and calculated using the ΔΔCt method as previously described (*12*).

In vitro RNA transcription

DNA templates for the in vitro transcription of scrambled RNA and *RNA5SP141* were generated by PCR as described previously (*12*) using KOD Hot Start Polymerase (EMD Millipore). DNA templates for the in vitro transcription of rabies virus leader sequence (RABVle) were generated by annealing sense and antisense oligonucleotides as previously described (*54*). RNA was synthesized using the MEGAshortscript In Vitro Transcription Kit (Ambion) and purified using the MEGAclear Transcription Reaction Purification Kit (Ambion). RNA integrity was evaluated with the Agilent 2100 Bioanalyzer System using the Small RNA Analysis Kit (Agilent).

In silico prediction of alternative transcriptional targets of TFIIIA

The human reference genome (hg38) was screened for potential binding sites of TFIIIA with the following promoter region: "TAAGCA.(15)AGTA.(7)GGGAGA." UROPA was used to annotate the recovered regions. In silico predictions were validated using a published transcription factor CHIP-seq dataset (ENCSR220AQM). In brief, HepG2 cells were used to perform TFIIIA CHIP-seq using the Illumina NovaSeq 6000 platform generated by the laboratory of R. Meyers (HudsonAlpha Institute for Biotechnology). Data presented were downloaded (www.encodeproject.org) and visualized using the "Integrative Genomics Viewer."

Statistics

Data were analyzed using a two-tailed Student's *t* test or one-way analysis of variance (ANOVA) test (as indicated), and *P* values of less than 0.05 were considered significant. Significant differences were denoted as $^{*}P < 0.05$, $^{**}P < 0.01$, $^{***}P < 0.001$, and $^{****}P < 0.0001$. Prespecified effect sizes were not assumed, and generally, three biological replicates (*n*) for each condition were used, unless otherwise indicated. Statistical analyses were performed using the Prism v9 software (GraphPad).

Supplementary Materials

This PDF file includes:
Case descriptions
Figs. S1 to S9
Tables S1, S2 and S4

Other Supplementary Material for this manuscript includes the following:
Table S3
Data file S1
MDAR Reproducibility Checklist

View/request a protocol for this paper from *Bio-protocol*.

REFERENCES AND NOTES

1. C. James, M. Harfouche, N. J. Welton, K. M. Turner, L. J. Abu-Raddad, S. L. Gottlieb, K. J. Looker, Herpes simplex virus: Global infection prevalence and incidence estimates, 2016. *Bull. World Health Organ.* **98**, 315–329 (2020).

2. R. J. Whitley, D. W. Kimberlin, Herpes simplex encephalitis: Children and adolescents. *Semin. Pediatr. Infect. Dis.* **16**, 17–23 (2005).
3. S. R. Paludan, A. G. Bowie, K. A. Horan, K. A. Fitzgerald, Recognition of herpesviruses by the innate immune system. *Nat. Rev. Immunol.* **11**, 143–154 (2011).
4. G. Liu, M. U. Gack, Distinct and orchestrated functions of RNA sensors in innate immunity. *Immunity* **53**, 26–42 (2020).
5. M. H. Orzalli, D. M. Knipe, Cellular sensing of viral DNA and viral evasion mechanisms. *Annu. Rev. Microbiol.* **68**, 477–492 (2014).
6. S.-Y. Zhang, E. Jouanguy, S. Ugolini, A. Smahi, G. Elain, P. Romero, D. Segal, V. Sancho-Shimizu, L. Lorenzo, A. Puel, C. Picard, A. Chapgier, S. Plancoulaine, M. Titeux, C. Cognet, H. von Bernuth, C.-L. Ku, A. Casrouge, X.-X. Zhang, L. Barreiro, J. Leonard, C. Hamilton, P. Lebon, B. Héron, L. Vallée, L. Quintana-Murci, A. Hovnanian, F. Rozenberg, E. Vivier, F. Geissmann, M. Tardieu, L. Abel, J.-L. Casanova, TLR3 deficiency in patients with herpes simplex encephalitis. *Science* **317**, 1522–1527 (2007).
7. S. Y. Zhang, J. L. Casanova, Inborn errors underlying herpes simplex encephalitis: From TLR3 to IRF3. *J. Exp. Med.* **212**, 1342–1343 (2015).
8. J. Rehwinkel, M. U. Gack, RIG-I-like receptors: Their regulation and roles in RNA sensing. *Nat. Rev. Immunol.* **20**, 537–551 (2020).
9. Y. Zhao, J. Karijolich, Know thyself: RIG-I-like receptor sensing of DNA virus infection. *J. Virol.* **93**, e01085-19 (2019).
10. A. Ablasser, F. Bauernfeind, G. Hartmann, E. Latz, K. A. Fitzgerald, V. Hornung, RIG-I-dependent sensing of poly(dA:dT) through the induction of an RNA polymerase III-transcribed RNA intermediate. *Nat. Immunol.* **10**, 1065–1072 (2009).
11. Y. H. Chiu, J. B. Macmillan, Z. J. Chen, RNA polymerase III detects cytosolic DNA and induces type I interferons through the RIG-I pathway. *Cell* **138**, 576–591 (2009).
12. J. J. Chiang, K. M. J. Sparrer, M. van Gent, C. Lässig, T. Huang, N. Osterrieder, K. P. Hopfner, M. U. Gack, Viral unmasking of cellular 5S rRNA pseudogene transcripts induces RIG-I-mediated immunity. *Nat. Immunol.* **19**, 53–62 (2018).
13. S.-Y. Zhang, N. E. Clark, C. A. Freije, E. Pauwels, A. J. Taggart, S. Okada, H. Mandel, P. Garcia, M. J. Ciancanelli, A. Biran, F. G. Lafaille, M. Tsumura, A. Cobat, J. Luo, S. Volpi, B. Zimmer, S. Sakata, A. Dinis, O. Ohara, E. J. Garcia Reino, K. Dobbs, M. Hasek, S. P. Holloway, K. McCammon, S. A. Hussong, N. DeRosa, C. E. Van Skike, A. Katolik, L. Lorenzo, M. Hyodo, E. Faria, R. Halwani, R. Fukuhara, G. A. Smith, V. Galvan, M. J. Damha, S. Al-Muhsen, Y. Itan, J. D. Boeke, L. D. Notarangelo, L. Studer, M. Kobayashi, L. Diogo, W. G. Fairbrother, L. Abel, B. R. Rosenberg, P. J. Hart, A. Etzioni, J.-L. Casanova, Inborn errors of RNA lariat metabolism in humans with brainstem viral infection. *Cell* **172**, 952–965.e18 (2018).
14. F. G. Lafaille, O. Harschnitz, Y. S. Lee, P. Zhang, M. L. Hasek, G. Kerner, Y. Itan, O. Ewaleifoh, F. Rapaport, T. M. Carlile, M. E. Carter-Timofte, D. Paquet, K. Dobbs, B. Zimmer, D. Gao, M. F. Rojas-Duran, D. Kwart, V. Rattina, M. J. Ciancanelli, J. L. McAlpine, L. Lorenzo, S. Boucherit, F. Rozenberg, R. Halwani, B. Henry, N. Amenzoui, Z. Alsum, L. Marques, J. A. Church, S. Al-Muhsen, M. Tardieu, A. A. Bousfiha, S. R. Paludan, T. H. Mogensen, L. Quintana-Murci, M. Tessier-Lavigne, G. A. Smith, L. D. Notarangelo, L. Studer, W. Gilbert, L. Abel, J.-L. Casanova, S.-Y. Zhang, Human SNORA31 variations impair cortical neuron-intrinsic immunity to HSV-1 and underlie herpes simplex encephalitis. *Nat. Med.* **25**, 1873–1884 (2019).
15. S. G. Tangye, W. Al-Herz, A. Bousfiha, C. Cunningham-Rundles, J. L. Franco, S. M. Holland, C. Klein, T. Morio, E. Oksenhendler, C. Picard, A. Puel, J. Puck, M. R. J. Seppänen, R. Somech, H. C. Su, K. E. Sullivan, T. R. Torgerson, I. Meyts, Human inborn errors of immunity: 2022 update on the classification from the international union of immunological societies expert committee. *J. Clin. Immunol.* , 1–35 (2022).
16. H. K. Lim, M. Seppänen, T. Hautala, M. J. Ciancanelli, Y. Itan, F. G. Lafaille, W. Dell, L. Lorenzo, M. Byun, E. Pauwels, Y. Rönnelid, X. Cai, S. Boucherit, E. Jouanguy, A. Paetau, P. Lebon, F. Rozenberg, M. Tardieu, L. Abel, A. Yildiran, A. Vergison, R. Roivainen, A. Etzioni, P. J. Tienari, J. L. Casanova, S. Y. Zhang, TLR3 deficiency in herpes simplex encephalitis: High allelic heterogeneity and recurrence risk. *Neurology* **83**, 1888–1897 (2014).
17. A. J. Oler, R. K. Alla, D. N. Roberts, A. Wong, P. C. Hollenhorst, K. J. Chandler, P. A. Cassiday, C. A. Nelson, C. H. Hagedorn, B. J. Graves, B. R. Cairns, Human RNA polymerase III transcriptomes and relationships to Pol II promoter chromatin and enhancer-binding factors. *Nat. Struct. Mol. Biol.* **17**, 620–628 (2010).
18. D. R. Engelke, S. Y. Ng, B. S. Shastry, R. G. Roeder, Specific interaction of a purified transcription factor with an internal control region of 5S RNA genes. *Cell* **19**, 717–728 (1980).
19. R. D. Little, D. C. Braaten, Genomic organization of human 5 S rDNA and sequence of one tandem repeat. *Genomics* **4**, 376–383 (1989).
20. J. Miller, A. D. McLachlan, A. Klug, Repetitive zinc-binding domains in the protein transcription factor IIIA from Xenopus oocytes. *EMBO J.* **4**, 1609–1614 (1985).
21. K. Kluska, J. Adamczyk, A. Krężel, Metal binding properties of zinc fingers with a naturally altered metal binding site. *Metallomics* **10**, 248–263 (2018).
22. M. Padjasek, A. Kocyła, K. Kluska, O. Kerber, J. B. Tran, A. Krężel, Structural zinc binding sites shaped for greater works: Structure-function relations in classical zinc finger, hook and clasp domains. *J. Inorg. Biochem.* **204**, 110955 (2020).
23. M. Ciganda, N. Williams, Eukaryotic 5S rRNA biogenesis. *Wiley Interdiscip. Rev. RNA* **2**, 523–533 (2011).
24. J. Vierna, S. Wehner, C. Höner zu Siederdissen, A. Martínez-Lage, M. Marz, Systematic analysis and evolution of 5S ribosomal DNA in metazoans. *Heredity* **111**, 410–421 (2013).
25. J. J. Hayes, T. D. Tullius, Structure of the TFIIIA-5 S DNA complex. *J. Mol. Biol.* **227**, 407–417 (1992).
26. K. J. Karczewski, L. C. Francioli, G. Tiao, B. B. Cummings, J. Alföldi, Q. Wang, R. L. Collins, K. M. Laricchia, A. Ganna, D. P. Birnbaum, L. D. Gauthier, H. Brand, M. Solomonson, N. A. Watts, D. Rhodes, M. Singer-Berk, E. M. England, E. G. Seaby, J. A. Kosmicki, R. K. Walters, K. Tashman, Y. Farjoun, E. Banks, T. Poterba, A. Wang, C. Seed, N. Whiffin, J. X. Chong, K. E. Samocha, E. Pierce-Hoffman, Z. Zappala, A. H. O'Donnell-Luria, E. V. Minikel, B. Weisburd, M. Lek, J. S. Ware, C. Vittal, I. M. Armean, L. Bergelson, K. Cibulskis, K. M. Connolly, M. Covarrubias, S. Donnelly, S. Ferriera, S. Gabriel, J. Gentry, N. Gupta, T. Jeandet, D. Kaplan, C. Llanwarne, R. Munshi, S. Novod, N. Petrillo, D. Roazen, V. Ruano-Rubio, A. Saltzman, M. Schleicher, J. Soto, K. Tibbetts, C. Tolonen, G. Wade, M. E. Talkowski, A. D. C. Genome, B. M. Neale, M. J. Daly, D. G. MacArthur, The mutational constraint spectrum quantified from variation in 141,456 humans. *Nature* **581**, 434–443 (2020).
27. M. Kondili, A. Fust, J. Preussner, C. Kuenne, T. Braun, M. Looso, UROPA: A tool for Universal RObust Peak Annotation. *Sci. Rep.* **7**, 2593 (2017).
28. H. Nailwal, F. K. Chan, Necroptosis in anti-viral inflammation. *Cell Death Differ.* **26**, 4–13 (2019).
29. The ENCODE Project Consortium, An integrated encyclopedia of DNA elements in the human genome. *Nature* **489**, 57–74 (2012).
30. E. Sjöstedt, W. Zhong, L. Fagerberg, M. Karlsson, N. Mitsios, C. Adori, P. Oksvold, F. Edfors, A. Limiszewska, F. Hikmet, J. Huang, Y. Du, L. Lin, Z. Dong, L. Yang, X. Liu, H. Jiang, X. Xu, J. Wang, H. Yang, L. Bolund, A. Mardinoglu, C. Zhang, K. von Feilitzen, C. Lindskog, F. Pontén, Y. Luo, T. Hökfelt, M. Uhlén, J. Mulder, An atlas of the protein-coding genes in the human, pig, and mouse brain. *Science* **367**, eaay5947 (2020).
31. M. U. Gack, Y. C. Shin, C. H. Joo, T. Urano, C. Liang, L. Sun, O. Takeuchi, S. Akira, Z. Chen, S. Inoue, J. U. Jung, TRIM25 RING-finger E3 ubiquitin ligase is essential for RIG-I-mediated antiviral activity. *Nature* **446**, 916–920 (2007).
32. S. S. Krishna, I. Majumdar, N. V. Grishin, Structural classification of zinc fingers: Survey and summary. *Nucleic Acids Res.* **31**, 532–550 (2003).
33. E. M. Jenkinson, M. P. Rodero, P. R. Kasher, C. Uggenti, A. Oojageer, L. C. Goosey, Y. Rose, C. J. Kershaw, J. E. Urquhart, S. G. Williams, S. S. Bhaskar, J. O'Sullivan, G. M. Baerlocher, M. Haubitz, G. Aubert, K. W. Barañano, A. J. Barnicoat, R. Battini, A. Berger, E. M. Blair, J. E. Brunstrom-Hernandez, J. A. Buckard, D. M. Cassiman, R. Caumes, D. M. Cordelli, L. M. De Waele, A. J. Fay, P. Ferreira, N. A. Fletcher, A. E. Fryer, H. Goel, C. A. Hemingway, M. Henneke, I. Hughes, R. J. Jefferson, R. Kumar, L. Lagae, P. G. Landrieu, C. M. Lourenço, T. J. Malpas, S. G. Mehta, I. Metz, S. Naidu, K. Õunap, A. Panzer, P. Prabhakar, G. Quaghebeur, R. Schiffmann, E. H. Sherr, K. R. Sinnathuray, C. Soh, H. S. Stewart, J. Stone, H. Van Esch, C. E. Van Mol, A. Vanderver, E. L. Wakeling, A. Whitney, G. D. Pavitt, S. Griffiths-Jones, G. I. Rice, P. Revy, M. S. van der Knaap, J. H. Livingston, R. T. O'Keefe, Y. J. Crow, Mutations in SNORD118 cause the cerebral microangiopathy leukoencephalopathy with calcifications and cysts. *Nat. Genet.* **48**, 1185–1192 (2016).
34. C. Uggenti, A. Lepelley, M. Depp, A. P. Badrock, M. P. Rodero, M.-T. El-Daher, G. I. Rice, S. Dhir, A. P. Wheeler, A. Dhir, W. Albawardi, M.-L. Frémond, L. Seabra, J. Doig, N. Blair, M. J. Martin-Niclos, E. Della Mina, A. Rubio-Roldán, J. L. García-Pérez, D. Sproul, J. Rehwinkel, J. Hertzog, A. Boland-Auge, R. Olaso, J.-F. Deleuze, J. Baruteau, K. Brochard, J. Buckley, V. Cavallera, C. Cereda, L. M. H. De Waele, A. Dobbie, D. Doummar, F. Elmslie, M. Koch-Hogrebe, R. Kumar, K. Lamb, J. H. Livingston, A. Majumdar, C. M. Lorenço, S. Orcesi, S. Peudenier, K. Rostasy, C. A. Salmon, C. Scott, D. Tonduti, G. Touati, M. Valente, H. van der Linden, H. Van Esch, M. Vermelle, K. Webb, A. P. Jackson, M. A. M. Reijns, N. Gilbert, Y. J. Crow, cGAS-mediated induction of type I interferon due to inborn errors of histone pre-mRNA processing. *Nat. Genet.* **52**, 1364–1372 (2020).
35. L. Naesens, J. Nemegeer, F. Roelens, L. Vallaeys, M. Meuwissen, K. Janssens, P. Verloo, B. Ogunjimi, D. Hemelsoet; Program for Undiagnosed Rare Diseases (UD-PrOZA), L. Hoste, L. Roels, M. De Bruyne, E. De Baere, J. Van Dorpe, A. Dendooven, A. Sieben, G. I. Rice, T. Kerre, R. Beyaert, C. Uggenti, Y. J. Crow, S. J. Tavernier, J. Maelfait, F. Haerynck, Mutations in RNU7-1 weaken secondary RNA structure, induce MCP-1 and CXCL10 in CSF, and result in Aicardi-Goutières syndrome with severe end-organ involvement. *J. Clin. Immunol.* **42**, 962–974 (2022).
36. J. L. Casanova, M. E. Conley, S. J. Seligman, L. Abel, L. D. Notarangelo, Guidelines for genetic studies in single patients: Lessons from primary immunodeficiencies. *J. Exp. Med.* **211**, 2137–2149 (2014).
37. Y. G. Chen, S. Hur, Cellular origins of dsRNA, their recognition and consequences. *Nat. Rev. Mol. Cell Biol.* **23**, 286–301 (2021).

38. B. Y. Nabet, Y. Qiu, J. E. Shabason, T. J. Wu, T. Yoon, B. C. Kim, J. L. Benci, A. M. DeMichele, J. Tchou, J. Marcotrigiano, A. J. Minn, Exosome RNA unshielding couples stromal activation to pattern recognition receptor signaling in cancer. *Cell* **170**, 352–366.e13 (2017).
39. N. Vabret, V. Najburg, A. Solovyov, P. Sulc, S. Balan, G. Beauclair, M. Chazal, H. Varet, R. Legendre, O. Sismeiro, R. Y. Sanchez David, C. McCLAIN, R. Gopal, L. Chauveau, O. Schwartz, N. Jouvenet, M. Markowitz, F. Tangy, N. Bhardwaj, B. D. Greenbaum, A. V. Komarova, Y RNAs are conserved endogenous RIG-I ligands across RNA virus infection and are targeted by HIV-1. *iScience* **25**, 104599 (2022).
40. J. H. Lee, C. Chiang, M. U. Gack, Endogenous nucleic acid recognition by RIG-I-like receptors and cGAS. *J. Interferon Cytokine Res.* **39**, 450–458 (2019).
41. R. de Reuver, E. Dierick, B. Wiernicki, K. Staes, L. Seys, E. De Meester, T. Muyldermans, A. Botzki, B. N. Lambrecht, F. Van Nieuwerburgh, P. Vandenabeele, J. Maelfait, ADAR1 interaction with Z-RNA promotes editing of endogenous double-stranded RNA and prevents MDA5-dependent immune activation. *Cell Rep.* **36**, 109500 (2021).
42. S. C. Eckard, G. I. Rice, A. Fabre, C. Badens, E. E. Gray, J. L. Hartley, Y. J. Crow, D. B. Stetson, The SKIV2L RNA exosome limits activation of the RIG-I-like receptors. *Nat. Immunol.* **15**, 839–845 (2014).
43. Q. Tang, R. E. Rigby, G. R. Young, A. K. Hvidt, T. Davis, T. K. Tan, A. Bridgeman, A. R. Townsend, G. Kassiotis, J. Rehwinkel, Adenosine-to-inosine editing of endogenous Z-form RNA by the deaminase ADAR1 prevents spontaneous MAVS-dependent type I interferon responses. *Immunity* **54**, 1961–1975.e5 (2021).
44. J. D. G. Jones, J. L. Dangl, The plant immune system. *Nature* **444**, 323–329 (2006).
45. M. E. Carter-Timofte, A. F. Hansen, M. Christiansen, S. R. Paludan, T. H. Mogensen, Mutations in RNA polymerase III genes and defective DNA sensing in adults with varicella-zoster virus CNS infection. *Genes Immun.* **20**, 214–223 (2019).
46. A. Ramanathan, M. Weintraub, N. Orlovetskie, R. Serruya, D. Mani, O. Marcu, P. Stepensky, Y. Weisblum, E. Djian, A. Shaag, S. Revel-Vilk, I. Fried, M. Kotler, A. Rouvinski, D. Wolf, O. Elpeleg, N. Jarrous, A mutation in POLR3E impairs antiviral immune response and RNA polymerase III. *Proc. Natl. Acad. Sci. U.S.A.* **117**, 22113–22121 (2020).
47. H. Abolhassani, L. Hammarström, C. Cunningham-Rundles, Current genetic landscape in common variable immune deficiency. *Blood* **135**, 656–667 (2020).
48. R. Pérez de Diego, V. Sancho-Shimizu, L. Lorenzo, A. Puel, S. Plancoulaine, C. Picard, M. Herman, A. Cardon, A. Durandy, J. Bustamante, S. Vallabhapurapu, J. Bravo, K. Warnatz, Y. Chaix, F. Cascarrigny, P. Lebon, F. Rozenberg, M. Karin, M. Tardieu, S. Al-Muhsen, E. Jouanguy, S. Y. Zhang, L. Abel, J. L. Casanova, Human TRAF3 adaptor molecule deficiency leads to impaired Toll-like receptor 3 response and susceptibility to herpes simplex encephalitis. *Immunity* **33**, 400–411 (2010).
49. W. Rae, J. M. Sowerby, D. Verhoeven, M. Youssef, P. Kotagiri, N. Savinykh, E. L. Coomber, A. Boneparth, A. Chan, C. Gong, M. H. Jansen, R. du Long, G. Santilli, I. Simeoni, J. Stephens, K. Wu, M. Zinicola, H. L. Allen, H. Baxendale, D. Kumararatne, E. Gkrania-Klotsas, S. C. Scheffler Mendoza, M. A. Yamazaki-Nakashimada, L. B. Ruiz, C. M. Rojas-Maruri, S. O. Lugo Reyes, P. A. Lyons, A. P. Williams, D. J. Hodson, G. A. Bishop, A. J. Thrasher, D. C. Thomas, M. P. Murphy, T. J. Vyse, J. D. Milner, T. W. Kuijpers, K. G. C. Smith, Immunodeficiency, autoimmunity, and increased risk of B cell malignancy in humans with *TRAF3* mutations. *Sci. Immunol.* **7**, eabn3800 (2022).
50. J. Jumper, R. Evans, A. Pritzel, T. Green, M. Figurnov, O. Ronneberger, K. Tunyasuvunakool, R. Bates, A. Žídek, A. Potapenko, A. Bridgland, C. Meyer, S. A. A. Kohl, A. J. Ballard, A. Cowie, B. Romera-Paredes, S. Nikolov, R. Jain, J. Adler, T. Back, S. Petersen, D. Reiman, E. Clancy, M. Zielinski, M. Steinegger, M. Pacholska, T. Berghammer, S. Bodenstein, D. Silver, O. Vinyals, A. W. Senior, K. Kavukcuoglu, P. Kohli, D. Hassabis, Highly accurate protein structure prediction with AlphaFold. *Nature* **596**, 583–589 (2021).
51. M. Varadi, S. Anyango, M. Deshpande, S. Nair, C. Natassia, G. Yordanova, D. Yuan, O. Stroe, G. Wood, A. Laydon, A. Žídek, T. Green, K. Tunyasuvunakool, S. Petersen, J. Jumper, E. Clancy, R. Green, A. Vora, M. Lutfi, M. Figurnov, A. Cowie, N. Hobbs, P. Kohli, G. Kleywegt, E. Birney, D. Hassabis, S. Velankar, AlphaFold Protein Structure Database: Massively expanding the structural coverage of protein-sequence space with high-accuracy models. *Nucleic Acids Res.* **50**, D439–D444 (2022).
52. F. Zeng, S. Zhang, Z. Hao, S. Duan, Y. Meng, P. Li, J. Dong, Y. Lin, Efficient strategy for introducing large and multiple changes in plasmid DNA. *Sci. Rep.* **8**, 1714 (2018).
53. G. Liu, J. H. Lee, Z. M. Parker, D. Acharya, J. J. Chiang, M. van Gent, W. Riedl, M. E. Davis-Gardner, E. Wies, C. Chiang, M. U. Gack, ISG15-dependent activation of the sensor MDA5 is antagonized by the SARS-CoV-2 papain-like protease to evade host innate immunity. *Nat. Microbiol.* **6**, 467–478 (2021).
54. T. Saito, D. M. Owen, F. Jiang, J. Marcotrigiano, M. Gale, Innate immunity induced by composition-dependent RIG-I recognition of hepatitis C virus RNA. *Nature* **454**, 523–527 (2008).

Acknowledgments: We thank the patients and their families for consenting to this research. We further acknowledge S. Humblet-Baron and the Adaptive Immunology Unit (KU Leuven) for providing experimental support for extended immunophenotyping on PBMCs. We thank D. Knipe (Harvard), W. J. Kaiser (Emory University), and N. Raab-Traub (UNC-Chapel Hill) for providing reagents. We thank M. Van Winckel, F. De Baets, and K. Claes for excellent clinical care and continuing support. **Funding:** This work was supported by the VIB Grand Challenge (VIB-UGent) and by U.S. National Institutes of Health grants AI165502 and AI087846 (to M.U.G.). L.N. and J.N. have received an FWO PhD fellowship. L.N. is a beneficiary of a Horlait-Dapsens grant. B.N.L. is supported by a European Research Council advanced grant (ERC-2017-ADG), a concerted research initiative grant from Ghent University (BOF/GOA/028), and an Excellence of Science (EOS) research grant (G0G2318N). T.K. is a senior clinical researcher at FWO. S.J.T. is a beneficiary of a postdoctoral FWO grant. J.M. was supported by an Odysseus II Grant (G0H8618N) from the Research Foundation Flanders (FWO) and by Ghent University. F.H. is supported by a BOF tenure track (UGent). R.B. is supported by the Research Foundation Flanders (FWO; G086521N), Ghent University (BOF19/GOA/004), and an EOS research grant (G0I1422N). **Author contributions:** Conceptualization: J.S., J.M., S.M., B.N.L., T.K., M.U.G., R.B., F.H., D.B., and L.N. Data curation: S.M., F.H., V.D., and L.N. Formal analysis: D.A., P.D.B., S.M., K.S., E.D.B., M.v.G., J.N., M.D.B., D.B., and L.N. Funding acquisition: J.M., B.N.L., M.U.G., R.B., F.H., and L.N. Investigation: D.A., S.J.T., P.D.B., S.M., J.-H.L., K.S., E.D.B., M.v.G., J.N., F.H., D.B., V.D., and L.N. Methodology: J.S., S.J.T., B.N.L., J.-H.L., K.S., G.L., J.N., M.U.G., F.H., V.D., and L.N. Resources: J.S., J.M., B.N.L., T.K., E.D.B., G.L., M.U.G., R.B., F.H., D.B., V.D., and L.N. Visualization: D.A., S.M., J.N., F.H., and L.N. Writing—original draft: S.J.T., M.U.G., F.H., and L.N. Writing—review and editing: D.A., S.J.T., S.M., B.N.L., E.D.B., M.D.B., M.U.G., R.B., F.H., D.B., and L.N. **Competing interests:** The authors declare that they have no competing interests. **Data and materials availability:** All sequence data pertaining to the proband and other family members are stored on the secured server of the Center for Medical Genetics Ghent according to privacy regulations. These sequence data are available to researchers upon approval of a specific request to the corresponding authors. All data needed to evaluate the conclusions in the paper are present in the paper or the Supplementary Materials.

Submitted 9 April 2022
Accepted 27 October 2022
Published 18 November 2022
10.1126/sciimmunol.abq4531

Science Immunology

GTF3A mutations predispose to herpes simplex encephalitis by disrupting biogenesis of the host-derived RIG-I ligand *RNA5SP141*

Leslie NaesensSantoshi MuppalaDhiraj AcharyaJosephine NemegeerDelfien BogaertJung-Hyun LeeKatrien StaesVeronique DebackerPieter De BleserMarieke De BruyneElfride De BaereMichiel van GentGuanQun LiuBart N. LambrechtJens StaalTessa KerreRudi BeyaertJonathan MaelfaitSimon J. TavernierMichaela U. GackFilomeen Haerynck

Sci. Immunol., 7 (77), eabq4531. • DOI: 10.1126/sciimmunol.abq4531

Another brick in the wall against herpes

A wide variety of host immune defenses are mobilized to contain human infection with the HSV-1 herpesvirus. Herpes simplex encephalitis (HSE) is a devastating form of HSV-1 infection that can indicate an underlying host immunodeficiency. Using whole-exome sequencing to search for a genetic etiology of HSE in a young boy, Naesens *et al*. discovered hypofunctional mutations in the *GTF3A* gene encoding the TFIIIA subunit of RNA polymerase III as the cause of impaired innate immunity to HSV-1. TFIIIA-mediated transcription of a host-derived noncoding ribosomal RNA contributes to activation of the RIG-I cytoplasmic RNA sensor and a type I interferon response contributing to HSV-1 control. These findings reveal another critical layer of innate defense that human cells use to control HSV-1 herpesvirus infections.